Physical Aging of Polylactide Based Graft Block Polymers

Ingrid N. Haugan,^{1,#} Bongjoon Lee,^{1,#} Michael J. Maher,¹ Aristotelis Zografos,¹ Haley J. Schibur,¹ Seamus D. Jones,^{1,2} Marc A. Hillmyer,³ and Frank S. Bates¹*

¹Department of Chemical Engineering and Materials Science, University of Minnesota, Minneapolis, MN 55455

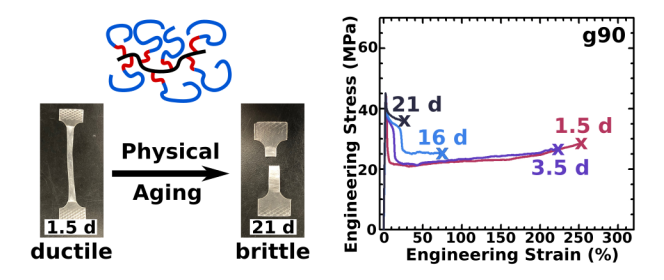
²Department of Chemical Engineering, University of California, Santa Barbara, Santa Barbara, CA 93106

³Department of Chemistry, University of Minnesota, Minneapolis, MN 55455

* To whom correspondence should be addressed: <u>bates001@umn.edu</u>

Co-first authors

TOC:



Keywords: Graft polymers, block copolymers, polylactide, sustainability, mechanical properties, physical aging, mechanical rejuvenation, pre-straining, shape memory

Abstract

Graft block polymers (BCPs) with poly(4-methylcaprolactone)-*block*-poly(±-lactide) (P4MCL-PLA) side chains containing 80 to 100% PLA content were synthesized with the aim of producing tough and sustainable plastics. These graft BCPs experience physical aging and become brittle

over time. For short aging times, t_a , the samples are ductile and shear yielding is the primary deformation mechanism. A double yield phenomenon emerges at intermediate t_a where the materials deform by stress whitening followed by shear yielding. At long t_a the samples become brittle and fail after crazing. PLA content strongly governs the time to brittle failure, where a 100% PLA graft polymer embrittles in 1 day, an 86% PLA graft BCP embrittles in 35 days, and at 80% PLA the material remains ductile after 210 days. Molecular architecture is also a factor in increasing the persistence of ductility with time; a linear triblock ages three times faster than a graft BCP with the same PLA content. SAXS and TEM analysis suggest that the rubbery P4MCL domains play a role in initiating crazing by cavitation. Pre-straining the graft BCPs also significantly toughens these glassy materials. Physical aging induced embrittlement is eliminated in all the pre-strained polymers, which remain ductile after aging for 60 days. The pre-strained graft BCPs also demonstrate shape memory properties. When heated above the glass transition temperature (T_g) the stretched polymer within seconds returns to its original shape and recovers the original mechanical properties of the unstrained material. These results demonstrate that graft BCPs can be used to make tough, durable, and sustainable plastics and highlight the importance of understanding the mechanical performance of sustainable plastics over extended periods of time following processing.

1. Introduction

Plastics are ubiquitous in today's society and have become a necessity in almost every aspect of life, from infrastructure to consumer and healthcare products. Of the more than 300 million tons of plastics that are produced each year, 90% came from non-renewable petroleum feedstocks. Furthermore, half of all plastics target single-use applications. Although convenient for everyday use, the end of life of these plastics are concerning: only 14% of plastics are collected for recycling and 72% end up in the environment or in landfills. Traditional, petroleum-derived plastics can have a lifetime of over 1000 years but may also degrade in UV light to form microand nanoplastics that can be environmentally detrimental. Biodegradable plastics offer pathways for plastics to break down into innocuous compounds, mitigating the mass accumulation of plastic waste. Polylactide (PLA) is a renewably sourced and biodegradable polymer that can be utilized as a strong plastic with a high elastic moduli. However, its use in many traditional applications is limited due to its inherent brittleness. Although PLA is initially tough when processed, it undergoes physical aging and becomes brittle over the course of 24 to 48 hours.

Physical aging can occur after polymers are rapidly cooled below their glass transition temperature, $T_{\rm g}$. ⁹⁻¹¹ The quenching process traps the polymer chains in a non-equilibrium, vitrified state; this glassy structure is metastable with excess free volume and relatively high molecular mobility as compared to the fully aged state. The increased molecular mobility allows polymer segments to rearrange through local relaxations (e.g., chain twisting) that reduce the excess free volume as the materials approaches, but never reaches, thermodynamic equilibrium. ¹² Evolution of the glassy structure during physical aging via structural relaxation results in changes to the potential energy landscape, which is related to the relative energy levels of the available deformation mechanisms activated when the polymer is subjected to macroscopic mechanical

stress. Theory and simulations have shown that the relative depth of the potential energy landscape basins increases with aging, altering the relative energetic costs associated with each deformation mechanism.¹³⁻¹⁷ These results have been replicated in laboratory experiments, which have shown that PLA typically transitions from ductile to brittle failure upon aging.^{8,18}

The inherent brittleness of neat PLA limits its applications, and thus significant effort has been expended to find methods of toughening this plastic. 19,20 Strategies to toughen PLA typically involve the addition of a rubbery component to favor energy dissipating deformation mechanisms, such as cavitation or shear yielding.²¹⁻²⁶ PLA containing block copolymers (BCPs) have been particularly successful at toughening PLA because they produce well-ordered and evenly dispersed rubber domains throughout the glassy matrix. The mechanical properties of these PLA BCPs depend on the volume fraction of PLA: materials with a minority of PLA content produce soft and highly ductile (E < 100 MPa, $\varepsilon_B > 500\%$) products, ²⁷⁻²⁹ while materials with high PLA content are stiff but less ductile (E > 1 GPa, $\varepsilon_B < 300\%$). Additionally, PLA BCPs typically require a high rubber content to significantly increase toughness,³¹ which reveals a balance between preparing plastics that are tough while still retaining the high strength of neat PLA. A graft architecture, where BCP side chains are attached to a common backbone, has been shown to further increase PLA toughness by physically connecting multiple domains.³²⁻³⁴ Graft polymers also have the added benefit of lower shear viscosities compared to linear polymers, making them more readily melt processable.35,36

Another method that can be used to obviate the effects of aging and toughen polymers is mechanical deformation, which can be understood by analogy with thermal processing.^{37,38} Heating a polymer above its T_g , or thermal rejuvenation, brings the polymer to an equilibrium, relatively high free volume state, and when the polymer is rapidly quenched the sample is trapped

in a metastable state that then undergoes physical aging. Mechanical deformation, or mechanical rejuvenation, has similarly been shown to increase the free volume and molecular mobility of polymers; when the mechanical strain is released, this metastable state also undergoes structural relaxation or physical aging. 15,39-46 Although the deformed material is brought to a higher free volume metastable state in both thermal and mechanical rejuvenation, the structure of the glassy state (i.e., potential energy landscape) for a mechanically rejuvenated polymer appears to be different than that of a thermally rejuvenated polymer. For example, the mechanically rejuvenated polymers typically exhibit a higher Young's modulus because the oriented polymer chains resist further extension. As a consequence, the dominant deformation mechanism of mechanically rejuvenated polymers differs from thermally rejuvenated polymers, favoring ductile deformation and effectively toughening the polymer. Although the mechanically deformed polymers exhibit a new glassy structure, studies have shown that the materials still undergo physical aging, evidenced by changes in mechanical properties with time. 48,49

While toughening of PLA by the addition of rubber components and physical aging of neat PLA have each been studied individually, there are few reports that address both approaches simultaneously. ^{18,50} In this work, we close this gap using PLA-based BCPs with linear and graft architectures. We describe the effects of physical aging on PLA toughening by combining three strategies: 1) varying the content of the rubbery component; 2) varying the polymer architecture; and 3) uniaxial pre-straining. We first discuss the model polymers and their bulk structure and mechanical properties, then describe the micromechanical deformation mechanisms of the polymers as a function of aging time. Embritlement during physical aging is compared to structural relaxation of the polymer glass as measured by differential scanning calorimetry. We then demonstrate how uniaxial pre-straining can be used to toughen PLA and mitigate physical

aging embrittlement. Finally, we demonstrate that the effects of pre-straining of the polymers are reversible and that these polymers exhibit shape memory behavior.

2. Materials and Methods

2.1 Materials

Poly[(styrene-*alt-N*-hydroxyethylmaleimide)-*random*-(styrene-*alt-N*-ethylmaleimide)]graft-[poly(4-methyl caprolactone)-*block*-PLA] graft BCPs were prepared as reported by Maher
et al.⁵¹ Linear triblock PLA-block-poly(4-methyl caprolactone)-block-PLA BCPs were prepared
by ring-opening transesterification polymerization as described by Watts et al.³⁰ Linear 100% PLA
(NatureWorks 4060D, 45.3 kg/mol) was purchased from NatureWorks. In all cases the polymers
were prepared using racemic (±) lactide monomer, resulting in amorphous PLA. Details of the
polymer synthesis are provided in the Supporting Information.

NMR spectra were recorded using a Bruker Advance III 500 MHz ¹H NMR and referenced to the solvent residual peak (CDCl₃, 7.26 ppm). Size exclusion chromatography (SEC) was performed on a Viscotek VE 2001 equipped with a VE 3580 RI detector and VE 270 dual detector. Two Varian PolyPore columns were employed (the linear polymers were characterized using three Varian PolyPore columns) operating at 40 °C with THF as the eluent flowing at a rate of 0.8 mL/min. A DAWN HELEOS multi angle light scattering detector and a dn/dc of 0.042 were used to determine absolute molecular weight. SEC traces for each model polymer are shown in Figure S1.

2.2 Tensile testing

Samples were hot pressed into thin films at 130 °C for 3 minutes using a Carver press (Wabash, IN) operated with a 200 μ m thick metal plate between Teflon sheets, then rapidly quenched to room temperature. After hot pressing, samples were cut into dog bone shaped tensile

bars using a Dumbbell Co, Ltd SDL-200 sample cutting machine equipped with a SDMK-1000 dumbbell cutter with dimensions of 5 mm width, 38 mm length, and 22 mm gauge length (according to ASTM D1708). Tensile bars were aged at ambient conditions (24 ± 2 °C) and the aging time was taken as the time between quenching and the start of testing. Uniaxial extension-to-break tests were conducted using a Shimadzu Autograph AGS-X Tensile Tester at room temperature with an extension rate of 1 mm/min following ASTM D1708. The Young's modulus (E) was calculated using the slope in the linear regime, from 0.1–1.5% strain for each sample. Samples that failed at visible defects or failed by tearing were not included in the data sets.

Pre-strained samples were prepared by stretching tensile bars to 200% strain at a rate of 1 mm/min in the tensile tester (samples were strained at aging times short enough that they only exhibited one yield point, as discussed below); after straining, the tensile bars were removed from the tensile tester and aged at ambient conditions, where the aging time was taken as the time between pre-straining and the start of testing. The dog bone specimens were cut isolating the gauge region and sandpaper was taped to the ends of the bar to use as grips. Pre-strained polymers had approximate dimensions of 3.0 mm width, 0.15 mm thickness, and 14 mm length. The pre-strained samples were then loaded into the tensile tester and strained to break at a rate of 1 mm/min. Analysis of the pre-strained polymers was performed in the same manner as the as-pressed samples. To test for shape memory, compression molded samples were pre-strained to 200%. After aging at ambient conditions for a specified time, the strained tensile bar was placed in an oven at 80 °C for 15 seconds, where the tensile bar recovered its original dog bone shape. The tensile bar was then aged at ambient conditions for a specified time and then strained to break at 1 mm/min.

2.3 Differential scanning calorimetry

Differential scanning calorimetry (DSC) was performed on a TA Instruments Discovery

DSC. Samples were hermetically sealed in aluminum pans under ambient conditions. The $T_{\rm g}$ was taken from the second heating scan from -90 to 200 °C at a rate of 10 °C/min. For the thermal annealing studies, samples were subjected to a heating cycle with varying annealing times, $t_{\rm a}$. Samples were first held at 100 °C for 2 minutes and quenched to 0 °C at 20 °C/min; the samples were then heated to 40 °C at 20 °C/min and annealed at 40 °C for various $t_{\rm a}$; the samples were then quenched to 0 °C at 20 °C/min and heated from 0 to 100 °C at 10 °C/min. The scans taken from 0 to 100 °C at 10 °C/min were used to evaluate the enthalpy overshoot of the annealed samples. This heating cycle is shown graphically in Figure S2.

2.4 Small-angle X-ray Scattering (SAXS)

SAXS data collected at the University of Minnesota Characterization Facility were used to determine bulk polymer morphology and SAXS data collected at Argonne National Laboratory were used to analyze crazes in strained polymers. The SAXS instrument at the University of Minnesota Characterization Facility used a photon wavelength of λ = 1.542 Å, a sample to detector distance of 1.05 m, and a Dectris Eiger 1M detector. SAXS data obtained at Argonne National Laboratory were collected on the DND-CAT 5ID-D beamline at the Advanced Photon Source using a sample to detector distance of 8.5 m, a photon wavelength of λ = 0.729 Å; 2D scattering patterns were collected using a Rayonix area CCD detector. NIKA software was employed for absolute intensity calibration (with corrections for sample thickness and exposure time) and reduction of two-dimensional scattering data into one-dimensional equatorial and meridional intensity data, where the equatorial intensities (perpendicular to the strain direction) and meridional intensities (parallel to the strain direction) were obtained by integration of the azimuthal angular range of $-5^{\circ} \leq \Phi \leq 5^{\circ}$ and $85^{\circ} \leq \Phi \leq 95^{\circ}$, respectively.

All SAXS samples were prepared using a method similar to that employed in generating

tensile testing samples, i.e., hot pressed at 130 °C and quenched to room temperature. To determine unstrained morphology, samples were cut directly from pressed films and mounted in a sample holder with Kapton tape. Strained and aged samples were first drawn in the tensile tester to a specified extension. Sections were then cut from the strained portions of the sample and mounted onto the stage with Kapton tape, positioning the sample such that the strain direction was approximately vertical.

2.5 TEM imaging

Samples were imaged using a Tecnai G2 Spirit Biotwin transmission electron microscope (TEM). Sample preparation followed the same procedure used to process the tensile testing specimens, i.e., hot pressed at 130 °C and quenched to room temperature. Unstrained samples were sectioned directly from pressed sheets, while samples strained in the tensile tester were sectioned in the deformed gauge section region. First, samples were cryo-microtomed with a glass knife on a Leica EM UC6 ultramicrotome operating at –120 °C (Model FC-S Cryo attachments) to create freshly cut surface. Then samples were bulk stained by exposing the freshly cut surface to the vapors of a RuO4 solution for 2 hours. Lastly, ultrathin cross-sectional slices (70 nm) were cut with a Diatome diamond knife on a Leica EM UC6 ultramicrotome operating at –120 °C (Model FC-S Cryo attachments). For pre-strained samples, sections were collected by cutting along the plane perpendicular to the thickness direction; the sample was cut parallel to the strain direction to distinguish between knife marks and features associated with sample deformation such as crazes. All samples were imaged at an operating voltage of 120 kV. Figure S19 illustrates the procedure used for TEM sample preparation.

3. Results and Discussion

3.1 Polymer synthesis

Model graft BCPs with high (80–100%) PLA content were prepared to study the effects of polymer composition and architecture on the mechanical properties and aging of these relatively stiff plastics. Poly(4-methyl caprolactone) (P4MCL) was used as the rubbery block because it has been shown to result in tough PLA plastics when incorporated into BCPs with PLA.³⁰ In addition, P4MCL is enzymatically degradable,⁵² making it a suitable candidate to pair with PLA for a sustainable alternative to traditional plastics. Scheme 1 shows the grafting-from synthesis of model graft BCPs with the chemical structure of poly[(styrene-*alt-N*-hydroxyethylmaleimide)-*stat*-(styrene-*alt-N*-ethylmaleimide)]-*graft*-(P4MCL-*block*-PLA). This synthetic strategy affords control over the grafting density, number of grafts, graft molar mass, and PLA volume fraction.⁵¹

Four model graft polymers were prepared with PLA volume fractions ranging from 0.8–1.0. Details on the synthesis and characterization data are provided in the Supporting Information; Table 1 lists the molecular characterization for all of the model polymers. All of the graft BCPs synthesized had a grafting density of 0.1 (defined as the average number of grafts per monomer unit in the backbone) and ranged from having 11–32 number averaged grafts per chain. For the graft polymers studied, the backbone volume fraction ranged from 1.7 to 2.4% assuming a backbone density of 1 g cm⁻³. Due to the low backbone content the reported volume fractions correspond to the composition of the grafts and ignore the contribution of the backbone. Two linear polymers were also studied to assess the effect of architecture. Linear PLA (NatureWorks 4060D) was purchased and used as received. Also, a linear PLA-P4MCL-PLA triblock (PLA volume fraction of 0.9) was prepared as described in the Supporting Information. The triblock was designed such that it would resemble a graft polymer with two grafts. In this report, the polymers

are named aXX, where a denotes the architecture (g for graft and l for linear), and XX refers to the PLA volume fraction of the grafts calculated based on PLA and P4MCL densities of 1.25 and 1.04 g/cm³ at 25 °C, respectively.³⁰ BCP will subsequently refer to all polymers that contain a P4MCL block and the architecture (graft/linear) will be specified when appropriate.

Scheme 1. Synthesis of model graft BCPs, poly[(styrene-*alt-N*-hydroxyethylmaleimide)-*stat*-(styrene-*alt-N*-ethylmaleimide)]-*graft*-[poly(4-methylcaprolactone)-*block*-poly(±-lactide)], using a grafting-from approach.

Table 1. Characterization data of PLA containing polymers

Sample	Number	M _{n,graft}	M _{n,graft}	$M_{\rm n,tot}$	%	$f_{\rm PLA}^{5}$	\mathbf{D}^3	$T_{ m g,P4MCL}$	$T_{ m g,PLA}$
ID	of	PLA ¹	P4MCL ²	(kg/mol) ³	backbone ⁴			(°C)6	(°C)6
	grafts	(kg/mol)	(kg/mol)						
g100	20	45		896	2.4	1.0	1.1		52
1100		45.33		45.3		1.0	1.5		55
g90	11	60	5.3	839	1.7	0.90	1.2	-59	52
190		75 ⁷	67	162	-	0.91	1.4	-64	51
g86	11	40	5.5	483	2.4	0.86	1.2	-51	50
g80	32	48	9.8	1450	1.9	0.80	1.3	-59	49

¹Number average molar mass, determined by % conversion in ¹H NMR ²Number average molar mass, determined by % conversion in ¹H NMR ³ $M_{\rm n}$ and dispersity were measured by SEC-MALS with a THF mobile phase ⁴% backbone is calculated by mass % ⁵ $f_{\rm PLA}$ is calculated assuming $\rho_{\rm P4MCL}$ = 1.04 g/cm³ and $\rho_{\rm PLA}$ = 1.25 g/cm³ at 25 °C, and ignores the backbone contribution ⁶Measured as the midpoint of the inflection in the transition from the second heating trace at a rate of 10 °C/min ⁷Triblock was synthesized to be analogous to a graft polymer with two grafts; to approximate the molar mass of the "graft" in the triblock $M_{\rm n,graft}$ is half of the total block molar mass of the polymer.

3.2 BCP Morphology

Figure 1 shows differential scanning calorimetry (DSC) traces for all of the polymers studied in this work. The BCPs show two T_g 's near -60 °C and 50 °C, corresponding to P4MCL and PLA, respectively. No T_g is observed for the poly[(styrene-*alt-N*-hydroxyethylmaleimide)-*stat*-(styrene-*alt-N*-ethylmaleimide)] backbone in any of the graft polymers, as is expected due to its low volume fraction. Due to the graft architecture, the backbone swells the P4MCL block (see below) and this likely contributes to the broad T_g observed for the rubbery domains. Lack of crystallization and melting peaks confirms that the polymers are completely amorphous (Figure S3). These results suggest that the BCPs are microphase separated into PLA and P4MCL rich domains.

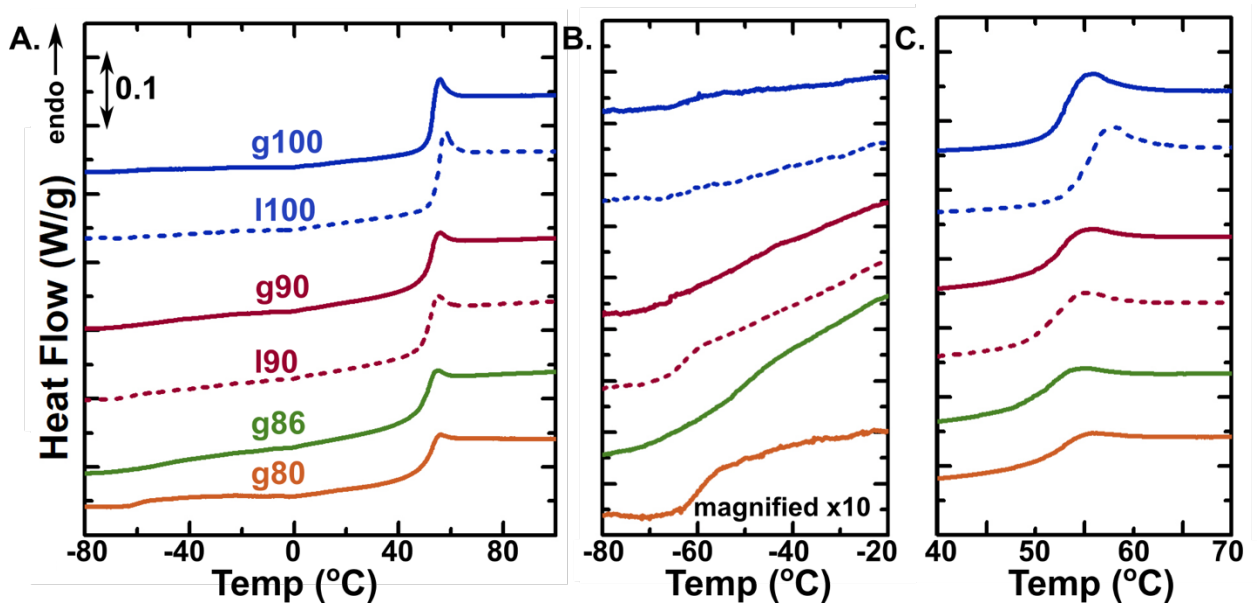


Figure 1. A. DSC traces for model polymers from -80 to 100 °C (traces are vertically shifted for clarity); data for graft polymers are shown using solid lines and data for linear polymers are shown using dashed lines. B. Expanded region of DSC trace from -80 to -20 °C to highlight the $T_{\rm g}$ of P4MCL, where the data are expanded by a factor of 10. C. DSC traces from 40 to 70 °C that highlight the $T_{\rm g}$ of PLA.

Figure 2 shows TEM images and SAXS traces for the polymers listed in Table 1 (except

the commercial PLA homopolymer), where staining with RuO₄ preferentially darkens the P4MCL rich domains. 53 The g100 graft polymer shows no features by TEM and no scattering peak in the SAXS trace, indicating that the backbone does not microphase separate from the side chains. The graft and linear BCPs appear by TEM to have well-defined microphase separated, quasi-spherical, rubbery domains. However, some rubbery domain interconnectedness is also evident, where the extent of interconnectivity appears to increase with P4MCL content. Whereas g90 displays only a small fraction of elongated rubber structures, g80 is characterized by a larger fraction of interconnected domains. Additionally, a comparison between the graft and linear BCPs with 90% PLA reveals that 190 shows more discrete P4MCL domains than g90. The SAXS traces (Fig. 2F) confirm microphase separation in all four graft block polymers, although the lack of higher-order peaks, along with the disordered morphology evident by TEM, indicates a lack of long-range order. The BCPs exhibit comparable domain spacings as measured by SAXS: 190, g90, g86, and g80 have primary scattering peaks at 0.17, 0.21, 0.27, and 0.26 nm⁻¹ respectively, corresponding to domain spacings of 36, 30, 24, and 24 nm. By TEM, 190 and g90 have rubber particle diameters of 7.4 ± 1.1 nm and 9.5 ± 1.2 nm (averaged over 100 particles), respectively. Although these two polymers have approximately the same PLA and P4MCL molar masses and PLA volume fraction, the diameter of the graft BCP rubber particles are within error of one another, but on average about 20% larger than the rubber particles for the linear counterpart. In addition, the rubber particles in the TEM images of all of the graft BCPs appear to occupy more volume than the molecular volume fraction of P4MCL. Both of these observations can be explained by swelling of the P4MCL particles with PLA and backbone chains. We speculate that due to the packing constraints of the graft architecture, the P4MCL chains are not able to adopt a conformation that fills space at bulk density while completely excluding the PLA chains, and as such, PLA chains may swell the rubber

domain to relax the conformational strain (depicted in Figure 2G). This interpretation is consistent with the broad glass transition associated with P4MCL in g90 and g86 as seen in Figure 1B.

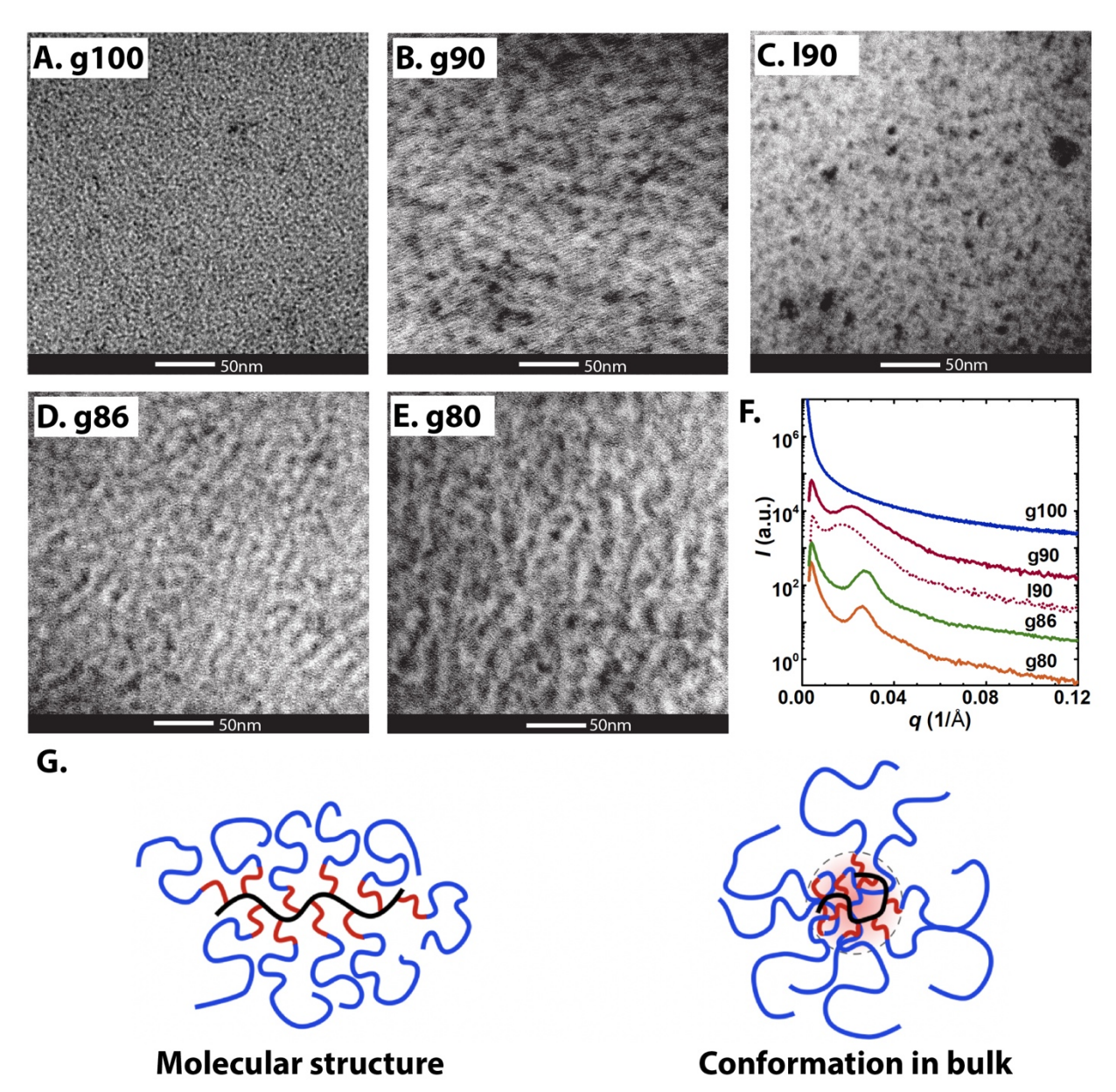


Figure 2. A-E. TEM images of model graft (g) and linear (l) block polymers, where the number denotes the overall volume fraction of PLA. F. SAXS traces for the polymers shown in panels A-E, where dashed lines indicate linear polymers and solid lines indicate graft polymers. G. Schematic showing the proposed molecular packing of g90, where PLA and backbone chains swell the rubber particles.

3.3 Mechanical properties of graft BCPs as a function of aging time

The addition of rubber and the use of the graft architecture have been shown to improve the toughness of PLA plastics.^{33,34} Although the mechanical properties of neat PLA have been shown to transition from ductile to brittle failure over the course of 24 to 48 hours,^{8,54} many reports of rubber toughened PLA plastics do not investigate the effects of physical aging and instead report a single (often unspecified) time point to represent the final mechanical properties of the materials. Herein, we test the tensile response of our model polymers over a range of aging times (from 1 hour to 210 days) to fully capture the development of their mechanical properties with aging time.

The mechanical properties were measured by uniaxial tensile experiments where the samples were pulled to failure after aging for various times, t_a . Figure S4 shows tensile curves for the polymers aged for 48 h (more than the time to brittle failure for neat PLA) and Table 2 gives a summary of the relevant mechanical properties. Linear and graft 100% PLA are both characterized by high moduli, with $E = 2.5 \pm 0.3$ and 2.9 ± 0.2 GPa, respectively, and low strain at break, less than 7% for each polymer. With 10% P4MCL, the strain at break increases several orders of magnitude to over 200% for both 190 and g90, and the modulus drops to 2.3 ± 0.1 and 2.1 ± 0.2 GPa for 190 and g90, respectively. The minor difference in moduli likely reflects the larger effective volume fraction of rubber in g90 due to mixing of PLA with P4MCL, and possibly some element of domain connectivity, as noted above. Increasing the amount of rubber drops the modulus further, where g86 and g80 have moduli of 1.9 ± 0.1 and 1.7 ± 0.1 GPa, respectively.

Table 2. Mechanical properties of PLA containing BCPs after aging 48 h at ambient conditions¹

Sample	E (GPa)	Toughness	$\sigma_{\!\scriptscriptstyle \mathrm{y}}$	<i>E</i> _y (%)	PYSD ²	$\sigma_{\!\scriptscriptstyle m b}$	& (%)	$G_{\rm R}^3$
ID		(MJ/m^3)	(MPa)		(MPa)	(MPa)		(MPa)
g100	2.9 ± 0.2	2 ± 1	52 ± 4	2.1 ± 0.1	4 ± 2	48 ± 4	4.6 ± 1.6	

1100	2.4 ± 0.1	2.8 ± 0.8	53 ± 2	2.6 ± 0.1	5 ± 1	47 ± 1	7 ± 2	
g90	2.1 ± 0.2	48 ± 10	45 ± 1	2.5 ± 0.2	19 ± 2	31 ± 3	230 ± 50	68 ± 10
190	2.3 ± 0.1	70 ± 30	50 ± 2	2.5 ± 0.1	19 ± 2	35 ± 3	210 ± 90	82 ± 4
g86	1.9 ± 0.1	85 ± 24	44 ± 2	3.0 ± 0.1	18 ± 2	36 ± 6	310 ± 50	85 ± 5
g80	1.7 ± 0.1	70 ± 3	37 ± 0.2	2.7 ± 0.2	15 ± 2	29 ± 3	296 ± 13	71 ± 3

¹Five replicates were performed for each sample and the values reported are the averages and standard deviations for each set ²Post-yield stress drop was taken as the difference in the yield stress and the plateau stress after the first yield point ³Strain hardening modulus, G_R , was taken as the slope of the stress-strain curve in the strain hardening regime, $\varepsilon > 200\%$

Figure 3 shows the tensile properties of each polymer as a function of aging time; Figure S5 shows the same tensile plots expanded from 0 to 40% to emphasize the changes in the low strain behavior. Figure S6 shows the strain at break, Young's modulus, yield stress, and post-yield stress drop as a function of t_a for all of the samples. Each polymer exhibits the same evolution of mechanical properties and deformation mechanism as they age, although across dramatically different time scales. This progression is divided into three aging regimes: short, intermediate, and long t_a regimes.

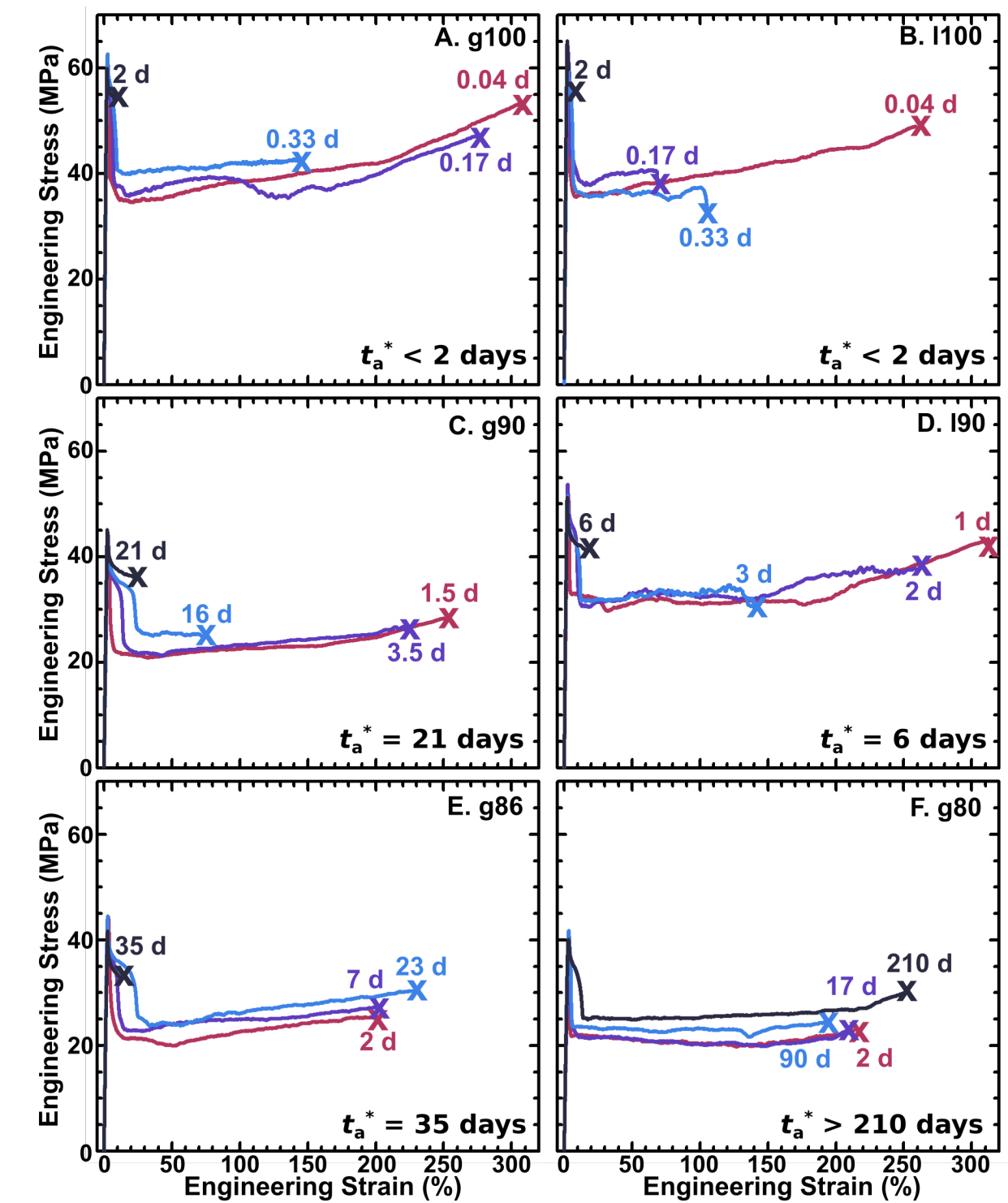


Figure 3. A-F. Tensile properties of model linear (l) and graft (g) polymers as a function of aging time (labeled on graph next to each curve) in ambient conditions, where the number following g or l denotes the overall volume fraction of PLA. The time to brittle failure, t_a^* , is labeled for each sample. Figure S5 shows the same tensile tests expanded from 0 to 40% strain to emphasize the differences in the low strain behavior.

Regime 1: In the short t_a regime the samples exhibit ductile deformation characterized by a single yield stress followed by shear yielding. Immediately after yielding diffuse shear bands form, coalescing into a single necked region. As the sample is stretched to higher strains the neck continuously propagates through the rest of the gauge region and the engineering stress becomes nearly invariant with increasing stress. Once the sample is fully cold-drawn at approximately 200% strain, the sample begins to strain harden and the engineering stress increases linearly with strain. The tensile bar remains optically clear for all of the samples throughout this deformation process, as shown in Figure S7.

Regime 2: The intermediate t_a regime is characterized by a double yielding phenomenon in the low strain region (<25% strain). After the first yield point the sample exhibits stress whitening within localized bands in the material (Figure S8),⁵⁵ which continues with additional strain until the second yield point, at which point the sample forms a stable neck that propagates by shear yielding upon further strain. In the early time portion of the intermediate t_a regime, the samples are able to fully cold draw to approximately 200% strain but do not extend into the strain hardening regime. As t_a increases within the intermediate regime, the onset of the second yield becomes delayed to higher strains and the strain at break decreases such that the polymer fails before being fully cold drawn.

Regime 3: In the long t_a regime the samples become brittle and break at low strain (<25% strain, as shown in Figure S9). The polymers exhibit crazing behavior (see below) with no shear yielding before brittle failure. The time for the sample to become brittle, i.e., enter regime 3, is defined as the time to brittle failure, t_a^* .

Although the same evolution of mechanical properties is observed for each polymer, t_a^* varies drastically between samples. The most important factor for setting t_a^* for these polymers

appears to be the PLA content: g100 (and l100) becomes brittle over the course of 2 days, whereas g86 embrittles after 35 days. Although the g80 sample appears to exhibit the short (regime 1) and intermediate (regime 2) aging characteristics, the sample does not become brittle on the time scales studied, hence $t_a^* > 210$ days. Architecture also appears to strongly influence the rate of aging. l90 becomes brittle after only 6 days, whereas g90 does not embrittle until it is aged for 21 days.

Previous reports have described a transition from shear yielding to crazing as PLA physically ages. 8,54 In general, polymers will deform by the lowest energy deformation mechanism, which is determined by the glassy structure (i.e., potential energy landscape) of the polymer. However, the glassy structure is continuously evolving with physical aging as the free volume in the polymer decreases. As a result, the relative energy levels of each deformation mechanism change with physical aging and the dominant deformation mechanism may change as well. As a polymer ages, it densifies and the polymer chains are brought closer together, thus reducing the free volume, which increases the van der Waals interactions between chains; increased interactions between chains increases the energy needed to separate polymer chains. In effect, the shear stress—the stress needed to shear yield—increases with physical aging, which is typically observed as an increase in the yield stress and Young's modulus. 56 In contrast, the craze stress is largely independent of aging time. 57

We postulate the following mechanism to explain the observed sequence of mechanical properties with aging. At short t_a , regime 1, the shear stress is lower than the craze stress and the material favors deformation by shear yielding. In regime 2—at intermediate times—the shear stress increases, becoming comparable to the stress required to craze, resulting in the observation of stress whitening and then shear yielding. At long t_a , regime 3, the shear stress exceeds the craze stress, and the material fails by rupture of craze fibrils before shear yielding can occur.

Another important factor that influences the deformation mechanisms with physical aging is strain localization. Minimal strain localization typically results in shear yielding and ductile deformation, whereas high strain localization typically leads to crazing and brittle failure.⁵⁸ The extent of strain localization depends on how the material responds to strain. Regions that strain harden will transfer local deformation to the surrounding matrix, resulting in a delocalization of strain. Materials that strain soften tend to concentrate stress into highly localized, weak regions of the plastic. It is well documented that strain softening and strain localization increase with physical aging,⁵⁸⁻⁶⁰ which is consistent with the transition from shear yielding to crazing that is reported here. Although strain softening can be monitored by the post-yield stress drop when testing in compression, we cannot use this quantity to evaluate our samples because all of the experiments were conducted in tension.

Physical aging of the rubber modified materials is more complicated, yet the same trend in deformation mechanisms emerges. First, it is important to understand how the rubbery domains alter the deformation mechanisms of the glassy matrix. For our BCPs, there are two main ways the rubbery domains toughen the PLA matrix: reduction of the shear stress and reduction of the craze stress. ⁶¹⁻⁶³ This is due to the fact that the rubber particles act as stress concentrators because stress localizes in the weakest part of the material. The stress concentration in the proximity of the rubbery particles also extends into the glass matrix, reducing the shear stress. The imposed stress field facilitates shear yielding of the glassy matrix because the stress field disrupts intermolecular interactions by introducing a repulsive force between segments, thereby reducing the shear stress. ⁶⁴ Stress concentrated in the rubber domains can also lead to cavitation of the particles, which may then serve as initiation points for crazing. Cavitation of rubber particles balances the energetic gain of relieving the internal stress of the rubber particle with the energetic cost of

creating a new surface between the rubber and the void.^{65,66} As a result, cavitation and subsequent crazing can occur once the imposed stress exceeds the energy needed to create a void.

For the BCPs, we speculate that the balance of shear yielding and crazing is determined by the propensity of the rubber particles to cavitate. We posit that at short aging times, the shear stress is lower than the cavitation stress, and the polymers shear yield before the rubber particles cavitate. However, at longer aging times the shear stress increases until shear yielding of the PLA requires more energy than rubber particle cavitation. We hypothesize that the rubber domains cavitate in the intermediate and long t_a regimes and subsequently initiate crazing.

We observe that t_a^* is strongly dependent on the volume fraction of the rubbery domain, which is consistent with other reports of physical aging of rubber toughened materials. 18,67,68 Although this trend is a function of composition, the suppression of embrittlement may also be due to the morphology of the BCPs. Wu previously reported that shear yielding was more favorable for rubber toughened systems with shorter interparticle distances. Wu attributed this to an increase in the strength of the stress field in the matrix with shorter interparticle distances, which would effectively decrease the shear stress more dramatically. From these results, we expect t_a^* for our PLA containing BCPs to inversely correlate with interparticle distance. This is indeed the case for some of our samples: 190, g90, and g86 had interparticle distances of 36, 30, and 24 nm and embrittle in 6, 21, and 35 days, respectively.

However, this explanation does not account for the vast difference in t_a^* between g86 and g80 (35 days and >210 days), which by SAXS analysis nominally have the same interparticle distance of 24 nm. We postulate that the interconnectedness of the polymers may be another significant factor in delaying the onset of stress whitening in our polymers. Work by Zhang *et al.* has shown that interconnected rubber structures, or network rubber morphologies, were

significantly more effective at toughening glassy matrices compared to discrete rubber particles.⁶⁹ They argued that a network rubber structure makes the induced stress field in the matrix more continuous and enables the delocalization of stress in the glassy matrix. However, the interconnected rubber domains also serve to weaken the material and lower the modulus. The BCPs in this report display a decrease in modulus with increasing interconnectivity (Table 2 and Figure S6B), indicating that our results are consistent with the conclusions drawn by Zhang *et al*. This effect of interconnectivity explains both the difference in t_a^* between 190 and g90 as well as the dramatic increase in t_a^* for g86 and g80. In general, the extent of interconnectivity seems to correlate with the time to brittle failure more consistently than the minor variations in interparticle distance.

3.4 Deformation mechanisms as a function of aging time

The mechanical data discussed above provide evidence of changes in the deformation mechanism as a function of aging time. TEM and SAXS were employed to further explore the micromechanical implications of these results for the BCPs in each aging regime. The g90 sample was selected as a model system for this purpose and was aged for three different t_a (corresponding to the three aging regimes) then strained to 10% to microscopically investigate the deformation of the BCPs during aging. All of the samples were strained *ex-situ* in the tensile tester and removed for TEM and SAXS analysis. The TEM samples were cut from the deformed sections of the tensile bars to produce ultrathin sections 70 nm thick and the samples were cut parallel to the strain direction in order to minimize artifacts from cryo-microtoming. The double-arrows in the TEM images denote the tensile strain direction; knife marks can be seen parallel to the strain direction

(see Figures S20–S22). SAXS analysis was performed on bulk samples, centered on the deformed portions of the gauge section of the tensile specimens.

In regime 1 the ductile polymers exhibit a single yield point (Figure 4A). TEM images of the necked region, highlighted by the yellow box in Figure 4B, are shown in Figure 4C-D. The low magnification TEM image (panel C) shows homogeneous deformation with no evidence of crazing, which is typically observed as either white or black lines perpendicular to the strain direction. High magnification TEM images (panel D) reveal that the rubber particles are aligned slightly along the tensile direction; this effect is not significant due to the small (10%) applied strain. The TEM images also reveal a lack of void formation in the P4MCL and PLA domains. This supports the mechanical data, where the samples deform solely by shear yielding.

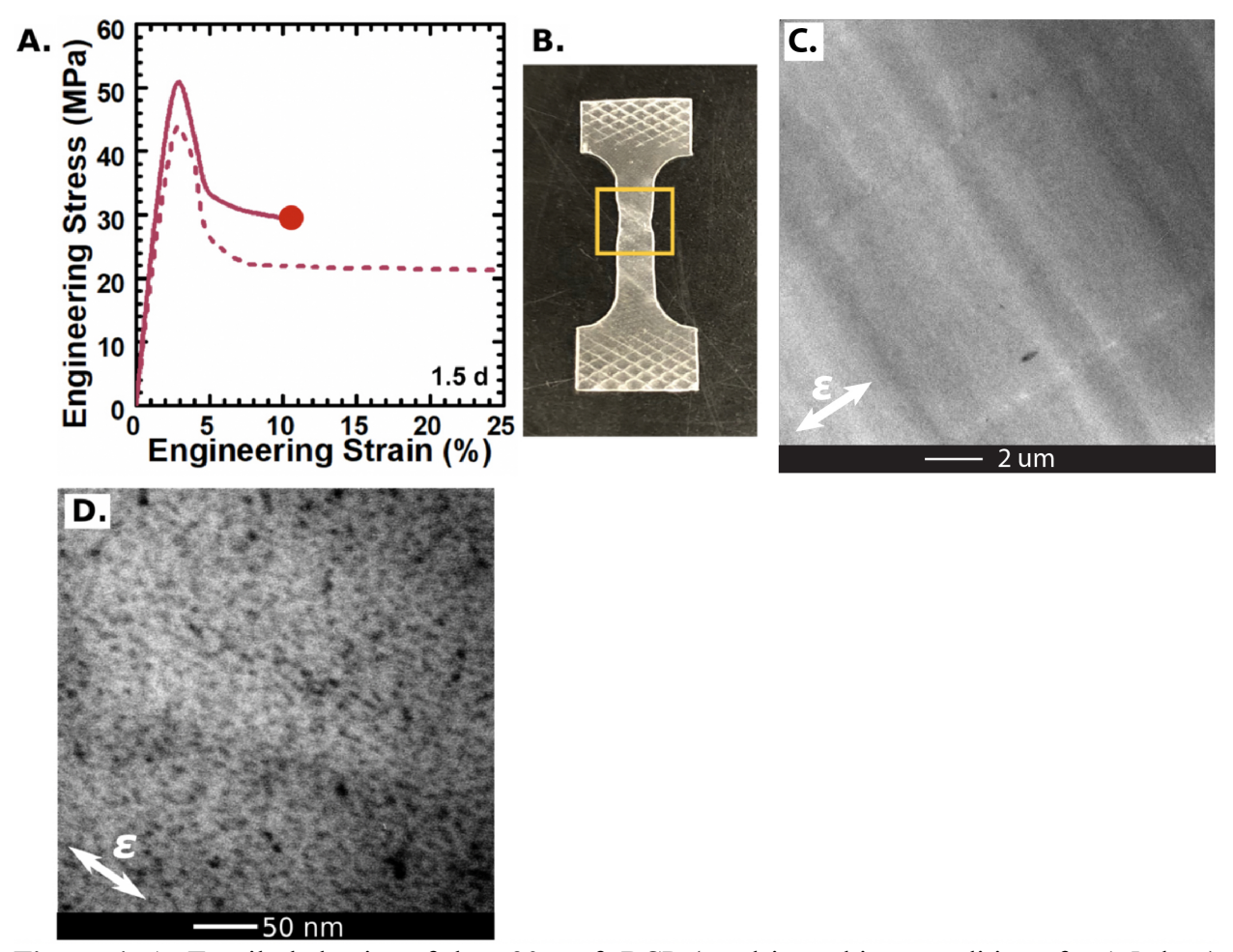


Figure 4. A. Tensile behavior of the g90 graft BCP (aged in ambient conditions for 1.5 days) pulled to 10% strain (indicated by the solid line and red dot) compared to the typical tensile behavior of g90 aged under the same conditions (dashed line and Figure 3C). B. Tensile bar after it was pulled to 10% strain; the region highlighted by the gold box was sectioned for analysis by TEM. C. TEM image of necked region highlighted in panel B; the double headed white arrow indicates the strain (ε) direction. The white lines are attributed to knife marks (see Figure S20) D. TEM image magnified to observe the morphology of the deformed region.

Regime 2 is characterized by the presence of a double yielding phenomenon, where the polymer whitens after the first yield point then necks at the second yield point, as a result of subsequent shear yielding. Figure 5A shows the tensile response of g90 after aging for 14 days. To analyze the behavior of the first yield, the sample was taken out of the tensile tester after straining to 10%, before the onset of the second yield point. TEM images of the gauge area, taken from the region highlighted by the yellow box in panel B of Figure 6, with varying magnification

are shown in panels C-F. In sharp contrast to regime 1, the TEM images of the sample aged for 14 days clearly show narrow bands of lower density material observed as white and black lines perpendicular to the tensile strain direction. At low magnification (panel C), the TEM image reveals arrays of these bands with an approximate widths of 50-400 nm. Higher magnification TEM images in panels D-F show their structure, which appears brighter than the surrounding area, which we interpret as voided material. The material outside of the bands appears to be undeformed, indicating that the deformation is localized to the voided region. Within these bands, which may be either crazes or deformation zones or shear bands, there are fewer rubber particles compared to the undeformed matrix.

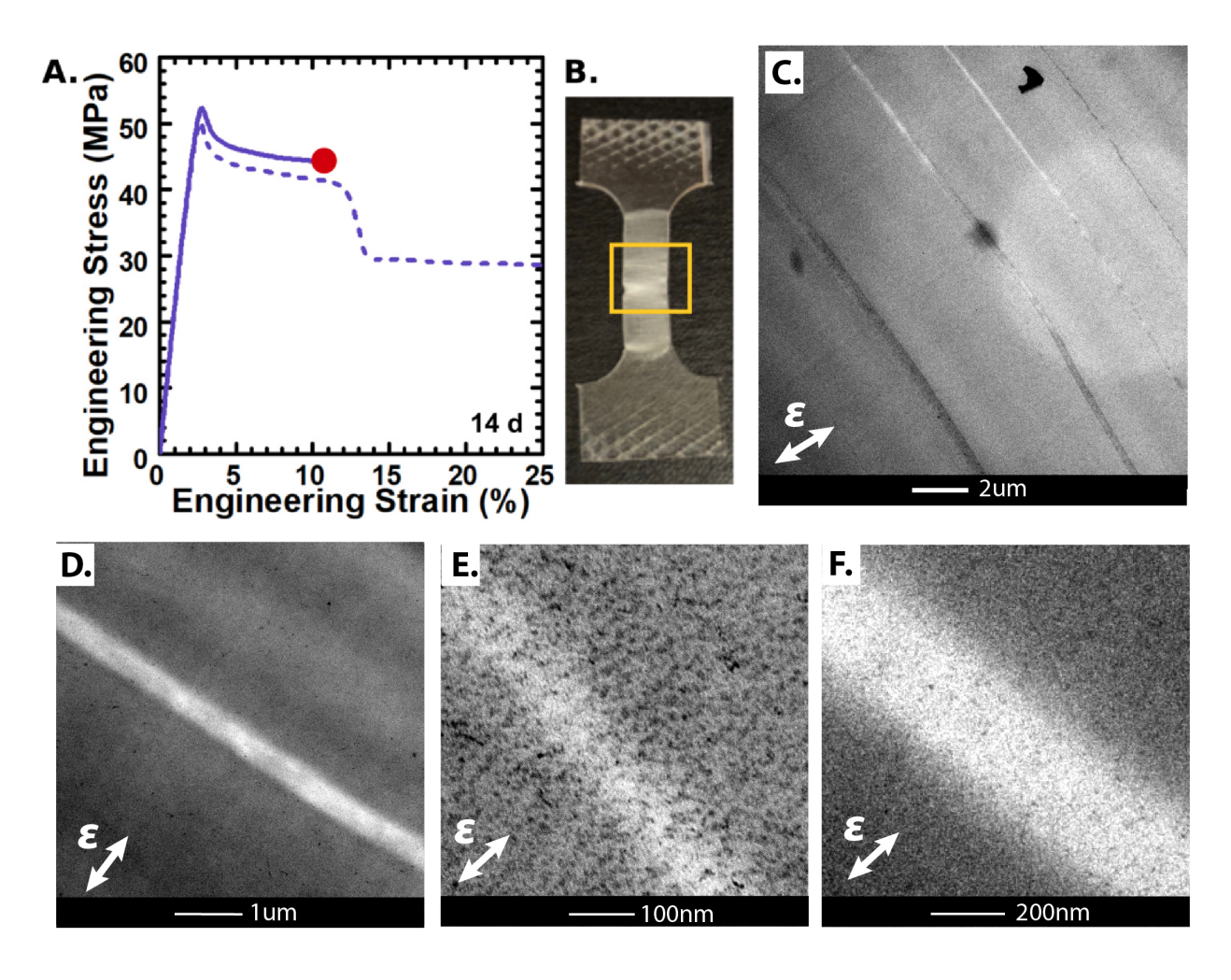


Figure 5. A. Tensile behavior of the g90 graft BCP (aged in ambient conditions for 14 days) pulled to 10% strain (indicated by the solid line and red dot) compared to the typical tensile behavior of g90 aged in the same conditions (dashed line and Figure 3C). B. Tensile bar after it was pulled to 10% strain; the region within the gold box was sectioned for analysis by TEM. C. Low magnification TEM image taken from the region highlighted in panel B. Shear bands are evident perpendicular to the strain direction. The double headed white arrow indicates the strain (ε) direction. D-F. Higher magnification TEM images of an individual craze.

Although the TEM images do not show clear evidence of rubber particle cavitation, SAXS results (see below) suggest that in fact the P4MCL rubber particles do cavitate, initiating either shear banding or crazing. Cavitation of rubber particles during craze formation has been previously reported. 66,70,71 Schwier *et al.* showed that polystyrene-*block*-polybutadiene (PS-PB) BCPs with cylindrical and spherical rubber morphologies produced crazing in the material under strain. 70,71 They observed cavitation of the polybutadiene domains within crazes surrounded by highly elongated polystyrene fibrils; the portions of the polymer outside of the craze remained undeformed and retained the original morphology. The cavitated material in sample g90 is restricted to much narrower bands than those reported by Schwier *et al.* This may be a consequence of the graft-block molecular architecture, which places significantly greater restrictions on the deformation and voiding of the rubber particles versus the PS-PB diblock copolymer architecture. Because the deformation bands are perpendicular to the direction of applied strain, we interpret them as crazes; shear bands form at $\pm 45^{\circ}$ relative to the applied tensile strain. 72

At long t_a in regime 3 the polymer produces a single yield point followed by evidence of crazing and brittle failure (Figure 6A and Figure 3C). TEM images obtained from the deformed gauge area, identified in Figure 6B, at various magnifications are shown in Figure 6C-F. The low magnification TEM image in panel C shows significant crazing, seen as black lines perpendicular to the strain direction. The features are markedly different than the ones produced in regime 2, being wider, ranging from 50 to 800 nm in width, and less uniform. Higher magnification TEM

images in panels D-F reveal striking features in the structure of these crazes (additional TEM images are shown in Figure S11). Similar to regime 2, the region outside of the craze appears to be undeformed (Figure S11C). However, in contrast to features in regime 2, the crazes have clear voids, greater than 100 nm in diameter, and large fibrils, or "macrofibrils," that span the entire craze. Macrofibril rupture can be seen in Figure 6E-F, where remnants are still present.

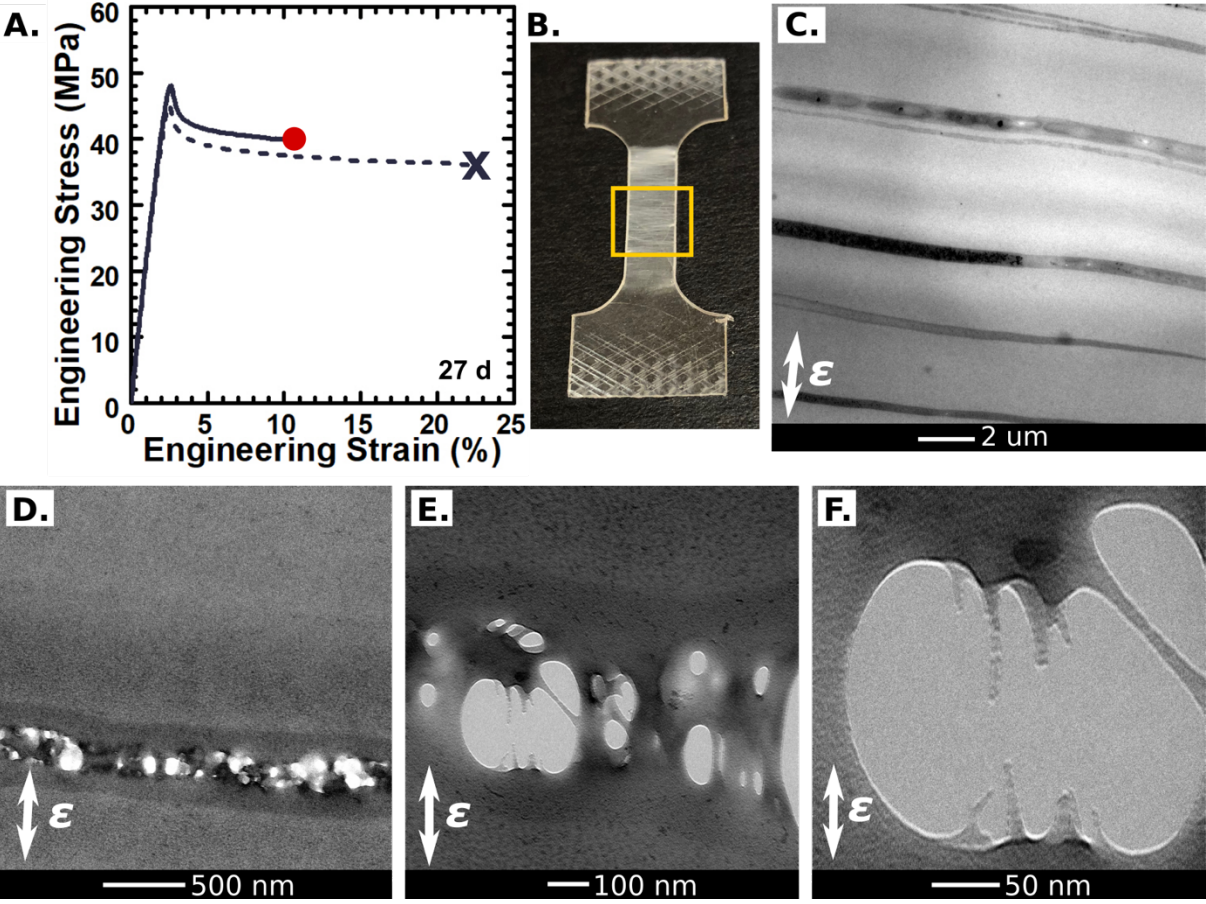


Figure 6. A. Tensile behavior of the g90 graft BCP (aged in ambient conditions for 27 days) pulled to 10% strain (indicated by the solid line and red dot) compared to the typical tensile behavior of g90 aged in the same conditions (dashed line and Figure 3C). B. Tensile bar after it was pulled to 10% strain; the region identified by the gold box was sectioned for analysis by TEM. C. TEM image of the region highlighted in panel B; the double headed white arrow indicates the strain (ε) direction. D-F. Magnified TEM images revealing the craze structure.

The deformation features in regimes 2 and 3 are dramatically different, which explains the qualitatively different mechanical properties of the material in these regimes. We hypothesize that

rubber particle cavitation occurs in both cases. The crazes formed in regime 2 contain mechanically robust PLA that can withstand the imposed deformation until the undeformed material outside of the craze starts shear yielding. However, the PLA fibrils formed in regime 3 are not mechanically stable enough to transfer the local stress to the surrounding undeformed material, which resists shear yielding due to aging. Fibril rupture leads to the formation of large voids, which spreads throughout the craze and leads to failure of the sample at low strains. The macrofibrils evident in panels D-F in Figure 6 also lack mechanical integrity resulting in sample failure at low strains without shear yielding.

While TEM provides detailed evidence of the morphological features of individual crazes, small-angle x-ray scattering (SAXS) offers complementary information on the behavior of the bulk samples. The anisotropic morphology of crazes yields characteristic 2D SAXS patterns. Figure 7 illustrates a 2D scattering pattern obtained from g90 after straining to 10% following 9 days of aging. The diffuse equatorial lobes along q_y centered around $q_x = 0$ arise from scattering from aligned fibrils with a characteristic inter-fibril distance, while the intense meridional streaks (along q_x centered at $q_y = 0$) are due to reflection from the surfaces formed by the crazes. Integration of the 2D scattering patterns in specific azimuthal ranges (85 to 95° for meridional scattering and -5 to 5° for equatorial scattering) yield 1D traces useful in quantifying the evolution of the deformation morphology.

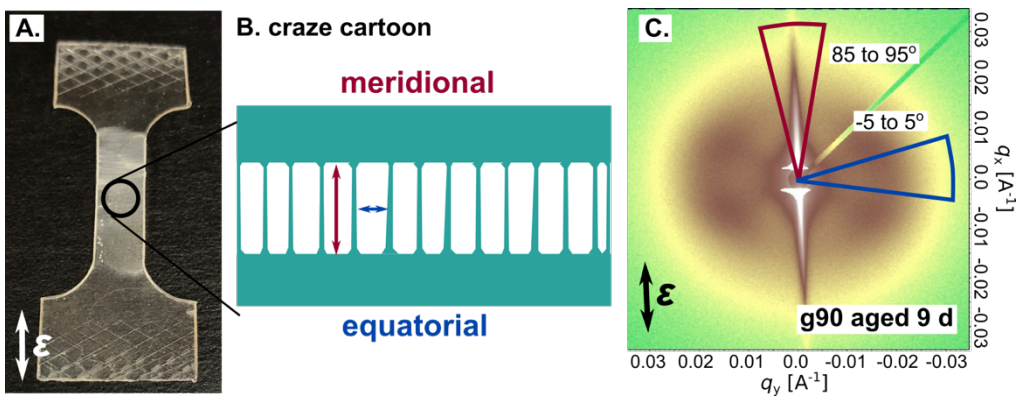


Figure 7. A. Tensile bar of g90 (aged 9 days in ambient conditions) after pulling to 10% strain, where the white double arrow indicates the strain (ε) direction. B. Schematic of an idealized voided shear band or craze demonstrating meridional and equatorial scattering from the structure. C. 2D SAXS pattern of tensile bar in panel A with schematics showing how the 2D data was integrated to obtain 1D traces for equatorial (blue pie slice, integrated from -5 to 5°) and meridional (red pie slice, integrated from 85 to 95°) scattering; the black double headed arrow indicates the strain direction.

Figure 8 shows the 2D scattering patterns for g90 aged at ambient conditions for varying times and strained to 10%. The samples were aligned such that the strain direction was approximately vertical, but the true strain direction is established by the direction of the meridional streak. Changes in the development and evolution of crazing in the sample are clearly evident as the material ages. After aging 1 day, relatively faint meridional scattering can be seen whereas the sample aged just 3 days shows intense meridional scattering intensity and well-defined large equatorial lobes. This is consistent with our mechanistic classification, where g90 is in regime 1 after aging 1 day and transitions to regime 2 after aging 3 days (Figure 3C). Both sets of features persist into regime 3 although the equatorial scattering intensity declines somewhat relative to the meridional scattering.

The SAXS patterns in Figure 8 are somewhat atypical relative to those normally associated with crazing. The equatorial scattering contains subtle lobes of intensity at azimuthal angles of about $\pm 25^{\circ}$ relative to the equatorial axis. These occur at q values consistent with the length scale of the morphology set by the spacing between the rubbery domains. We do not know the origins

of this scattering but speculate that it is associated with constraints imposed by the graft block molecular architecture.

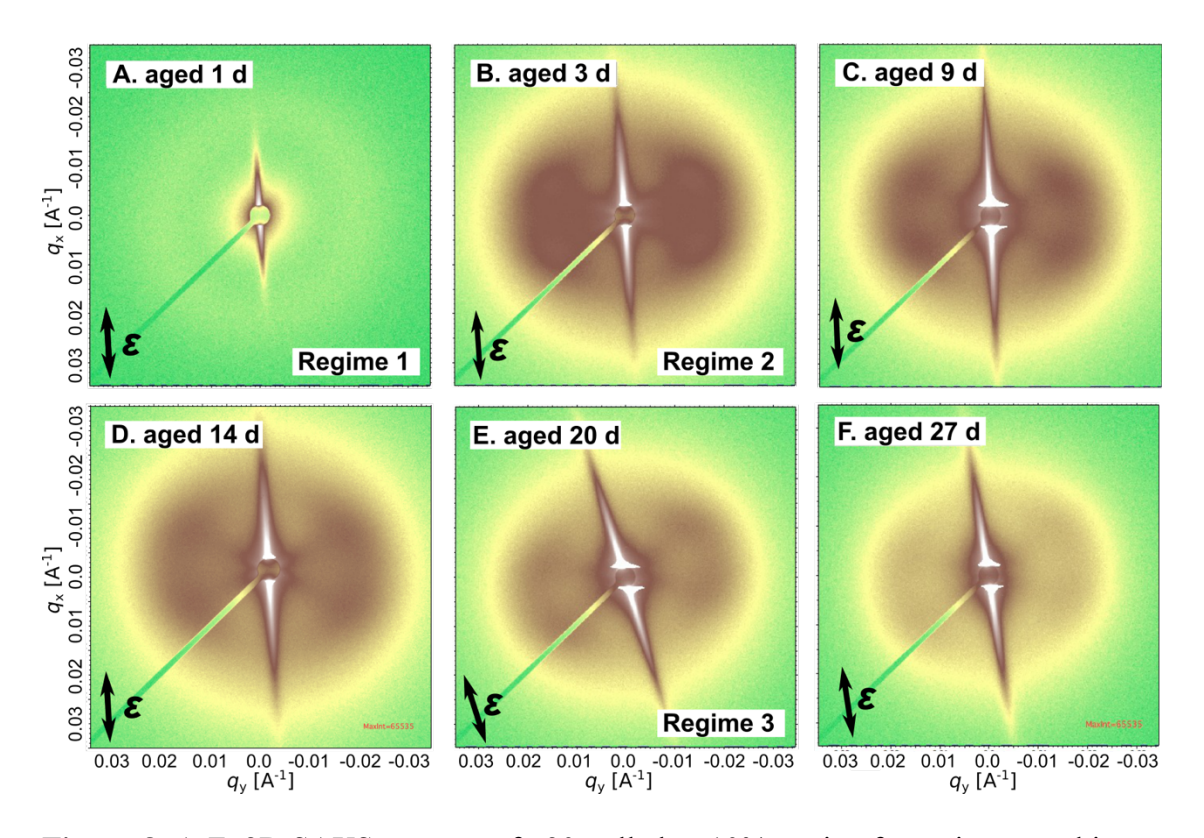


Figure 8. A-F. 2D SAXS patterns of g90 pulled to 10% strain after aging at ambient conditions. The three aging regimes for g90 are labelled in the lower right corner at the appropriate aging times. The black double-sided arrow indicates the strain (ε) direction, which is coincident with the direction of the meridional scattering streaks.

Figure 9 shows the 1D meridional and equatorial scattering traces obtained from integrating the 2D SAXS patterns in Figure 8; for reference, the dashed black line in both plots shows the scattering from an undeformed g90 sample. The sample aged 1 day shows almost identical equatorial scattering to the undeformed sample (a ring of intensity at q = 0.021 Å⁻¹ in Figure 8A), along with modest meridional scattering at low q. Development of a meridional streak suggests that the sample forms some crazes in regime 1, but the low meridional scattering intensity and the weak and isotropic equatorial scattering indicates that the overall density of these features

must be very low, consistent with the absence of deformation bands in the associated TEM images and with shear yielding being the dominant deformation mechanism in regime 1 at short t_a . After aging for 3 days or more, the scattering intensity increases dramatically in both the equatorial and meridional directions, which we associate with the formation of crazes based on the TEM and SAXS results shown in Figures 5 and 8, respectively. In the equatorial direction the scattering intensity after 3 days of aging increases by about 2 orders of magnitude while retaining a peak at $q = 0.017 \text{ Å}^{-1}$ (spacing of 36 nm) which is slightly reduced from that evident in the undeformed sample at $q = 0.021 \text{ Å}^{-1}$ (spacing of 30 nm). This observation is consistent with void formation (e.g., cavitation), which leads to a steep increase in the electron density contrast between the particles and matrix polymer. 75 Based on the near coincidence between the peak scattering before and after straining, we believe that the microstructure templates crazing through cavitation of the rubbery domains. The intensity of the equatorial scattering drops in regime 3 (i.e., 27 days in Figure 9A) consistent with an increase in the number of crazes with large voids, which would decrease the total number of equatorial scattering sites. However, the relatively constant intensity of the meridional scattering found in Figure 9B between 3 and 27 days of aging suggests that the total level of crazing remains relatively constant.

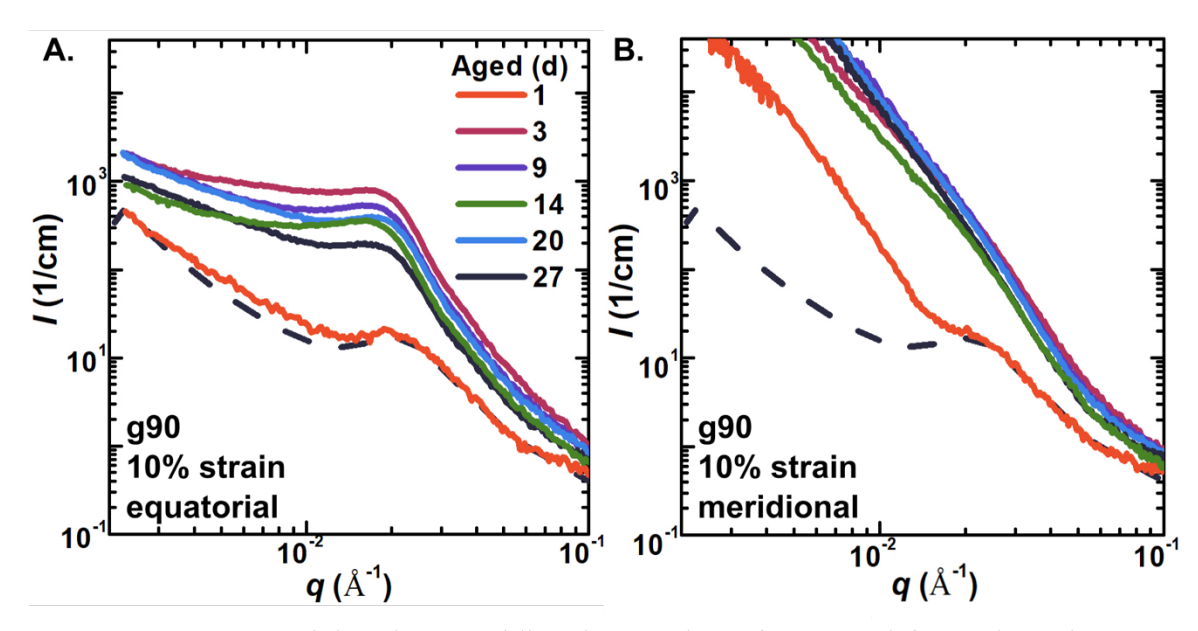


Figure 9. A. Equatorial and B. meridional scattering of g90 aged for various times at ambient conditions, then stretched to 10% strain (solid lines). The dashed black line was obtained from the undeformed material.

3.5 Assessment of physical aging by differential scanning calorimetry

Up to this point we have demonstrated the consequences of physical aging through changes in the mechanical properties with aging time. As discussed previously, the mechanical properties depend on numerous effects: although these observed changes occur as physical aging proceeds, they may not be *solely* due to the structural relaxation of polymer chains that is the crucial component of physical aging. DSC experiments were conducted to further explore how changes in the composition and molecular architecture affect evolution of the glassy state and whether these parameters independently affect the rate of structural relaxation.

Physical aging densifies the glassy structure of the polymer. Transitioning from the glassy state to the liquid state requires more energy for densified polymer chains, which manifests as an enthalpic overshoot at T_g . The extent of physical aging can be quantified by the area under the curve of the enthalpic overshoot. We annealed all the samples in the DSC at 40 °C to accelerate the rate of aging, allowing significant aging to occur in less than 8 hours. As a result, the aging

times in the mechanical testing and the aging times in the DSC studies cannot be directly compared. To assess the enthalpy overshoot, the polymers were subjected to a controlled thermal history, as described in the Methods and Materials section. A final heating ramp from 0 to 100 °C at 10 °C/min was used to observe the enthalpy overshoot.

Figure 10 shows the heating traces for all the polymers studied, where the enthalpy for each heating trace was normalized by the PLA content. All of the polymers showed the development of an enthalpy overshoot at $T_{\rm g}$, with the magnitude of the enthalpy overshoot increasing with increasing t_a . For the same aging conditions, the 100% PLA polymers had a higher extent of aging compared to the BCPs, as observed by a larger area under the enthalpy curves for g100 and 1100. Reduction of the rate of structural relaxation by the addition of rubber components has been reported previously, 18 consistent with the mechanical data, where the 100% PLA polymers embrittled much faster than the P4MCL containing polymers. Although the addition of P4MCL appeared to reduce the extent of aging for the same annealing conditions, the amount of rubber does not appear to significantly affect the aging rate of the glassy PLA as measured by DSC. Additionally, architecture does not appear to influence structural relaxation of the polymers, i.e., 190 and g90 produce virtually identical results. Both of these observations contrast with the mechanical data, where both composition and architecture strongly dictated the rate of embrittlement. These results suggest that the rubbery domains change the glassy structure but that variations in chain connectivity and rubber domain morphology do not appreciably affect structural relaxation of the glassy PLA. Instead, the mere presence or absence of the rubbery particles appears to be the most important factor in changing the rate of structural relaxation.

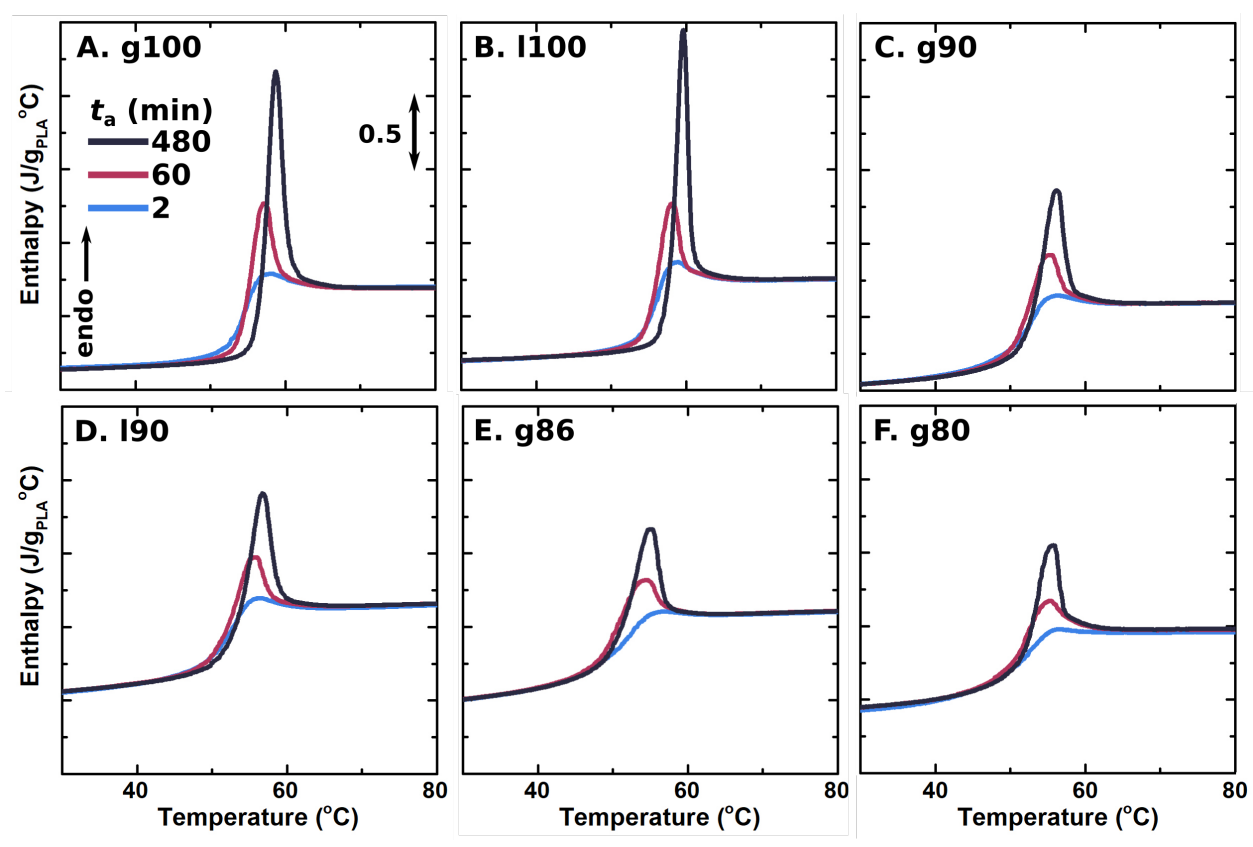


Figure 10. A-F. DSC traces, normalized for PLA content, after aging at 40 °C for various times.

It is important to note that although g80 did not embrittle over the timescales studied (< 210 days), it *did* experience structural relaxation by physical aging, as indicated by the evolution of an enthalpic overshoot (Figure 10F). This underscores the fact that the addition of rubber does not prevent physical aging of the glassy domains; instead the rubbery domains interact with the PLA in other ways to reduce the effects of physical aging on the mechanical properties (i.e., reducing the shear stress). This observation emphasizes that the mechanical response of the PLA materials as a function of aging time is not a single function of the extent of densification. Instead the mechanical response is a complex process dictated by several factors (e.g., relative deformation energies and strain localization).

3.6 Pre-strained polymers

The use of rubbery domains and a graft block architecture facilitate ductile deformation in PLA and delay transition of the material from being ductile to brittle. With the goal of producing tough PLA plastics that retain their ductility indefinitely, we explored an alternative approach. Mechanical pre-straining has been shown to improve the mechanical properties of hard plastics, increasing their strength and ductility. The improved strength of these pre-strained polymers is generally attributed to the orientation of the polymer chains because the elongated polymer chains resist further deformation. We pre-strained the materials by uniaxially stretching tensile bars at a strain rate of 1 mm/min at ambient conditions. All of the samples were pre-strained in regime 1, i.e., at short t_a , such that they exhibited a single yield point with ductile deformation (i.e., g90 was pre-strained after aging for < 1 day whereas g100 was pre-strained after aging only 1 hour).

The morphology of the pre-strained g90 was examined by TEM and SAXS to understand how the molecular conformation changes with deformation (Figure 11). The TEM images demonstrate that the rubber particles affinely deform along the tensile direction with no evidence of crazing or cavitation. SAXS analysis shows that large equatorial lobes arise with deformation, where the intensity of the scattering increases with increasing deformation. The equatorial scattering was due to the scattering between extended rubbery domains perpendicular to the strain direction. The absence of intense meridional scattering evidences that no crazes are present in the samples.

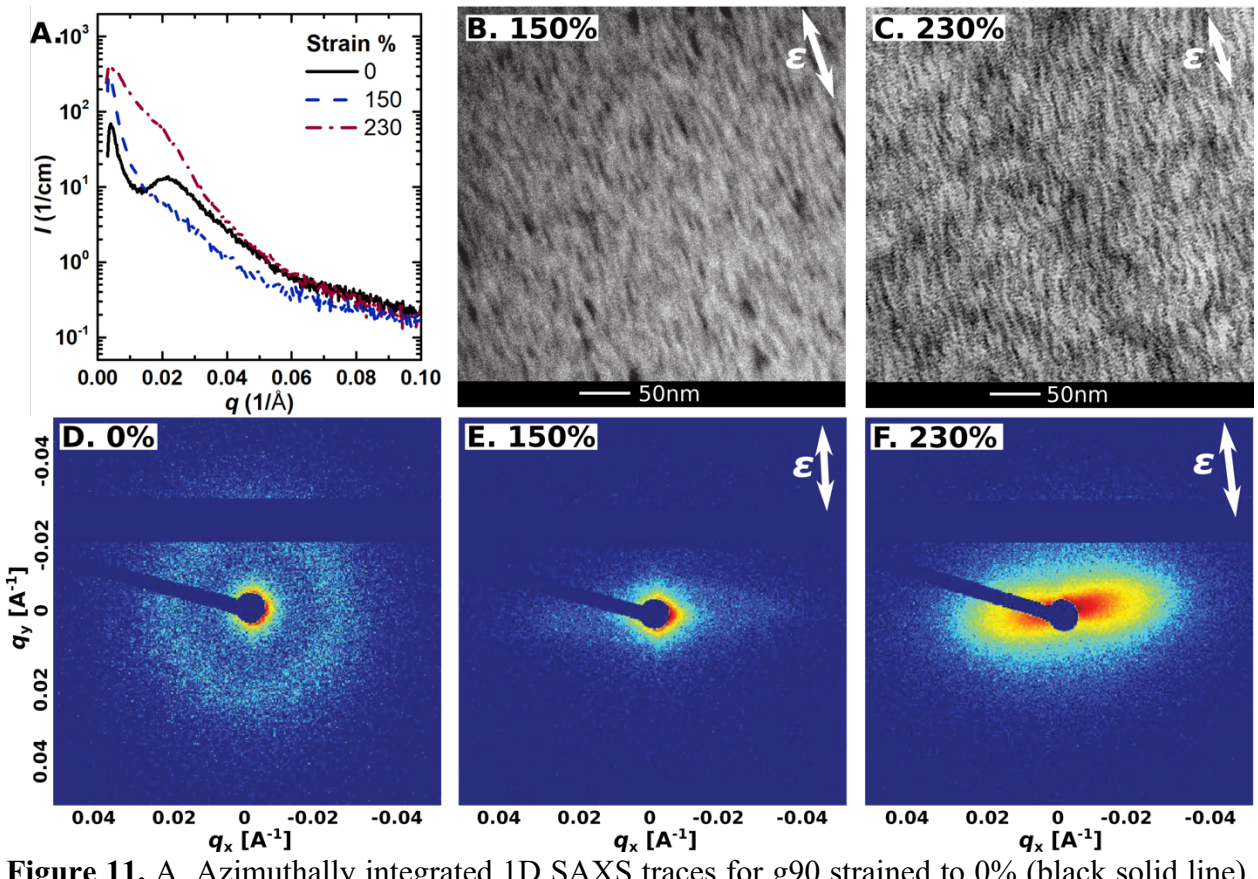


Figure 11. A. Azimuthally integrated 1D SAXS traces for g90 strained to 0% (black solid line), 150% (blue dashed line), and 230% (red dash-dot line). B-C. TEM images of g90 at 150 and 230% strain. D-F. 2D SAXS patterns for g90 at 0, 150, and 230% strain. All samples were aged <1 day at ambient conditions before straining; the white double-headed arrow indicates the strain direction.

Pre-strained polymers for mechanical testing were prepared by straining the regime 1 tensile bars to 200% strain, followed by cutting out a section from the strained gauge section to create a new tensile specimen (Figure S12). The mechanical properties of the pre-strained polymers were tested by uniaxial extension-to-break experiments at 1 mm/min. Figure 12 shows the representative tensile behavior for each polymer and the averaged results are summarized in Table 3. These results are compared to the as-pressed samples that were aged for 48 hours (Figure S4 and Table 2), which is the reported time for neat PLA to embrittle and as such is taken as the typical time that PLA materials are aged.^{8,18} The pre-strained polymers deform elastically at low

strains, then undergo yielding and subsequent strain hardening. Overall, pre-straining improves all the measured mechanical properties. This is consistent with previous results for pre-strained PLA. 80,83,84 However, previous reports strained PLA above $T_{\rm g}$ whereas all of the polymers in this report were pre-strained below $T_{\rm g}$. All of the pre-strained polymers have a higher modulus and higher yield stress compared to the as-pressed counterparts. For example, when pre-strained, the modulus and yield stress for g100 increase 20% (2.9 to 3.7 GPa) and 100% (50 to 100 MPa), respectively, compared to the as-pressed sample, and the tensile strength rises more than 3-fold (see Figure 3B). Moreover, the materials exhibit significant ductility: all of the samples break at greater than 40% strain, including the 100% PLA materials. Pre-straining also imparts significant toughening of the polymers: the pre-strained g100 has a tensile toughness of 48 MJ/m³, 24 times greater than the aspressed tensile toughness of 2 MJ/m³. In fact, pre-straining the g100 sample yields the same tensile toughness as the as-pressed g90 sample, but with a higher modulus. In effect, pre-straining toughens the PLA materials without sacrificing strength, a common tradeoff with rubber toughened materials.

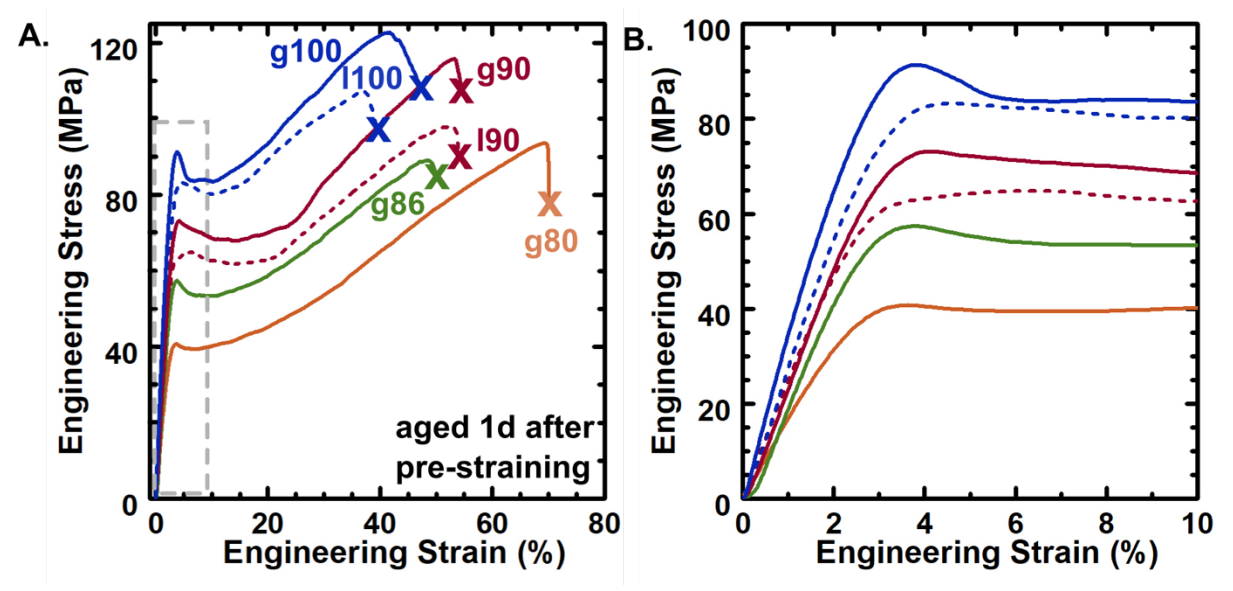


Figure 12. Representative tensile curves of pre-strained polymers (strained to 200%, aged at ambient conditions, and then strained to break; see Figure S13 for all replicates). Samples were pre-strained at short aging time (such that the sample exhibited only shear yielding with no crazing)

and aged 1 day at ambient conditions after pre-straining. A. Full strain range, with a grey box surrounding the low strain region highlighted in B.

Table 3. Mechanical properties of pre-strained PLA polymers¹

Sample	E (GPa)	Toughness	$\sigma_{\!\scriptscriptstyle m V}$	ε _ν (%)	PYSD ²	$\sigma_{ m b}$	& (%)	$G_{\rm R}^3$
ID		(MJ/m^3)	(MPa)	• ` `	(MPa)	(MPa)	, ,	(MPa)
g100	3.7 ± 0.6	48 ± 8	103 ± 9	3.8 ± 0.3	8 ± 2	135 ±11	46 ± 8	191 ± 70
1100	2.7 ± 0.1	35 ± 8	79 ± 7	4.5 ± 0.4	1 ± 1	112 ± 11	39 ± 6	131 ± 20
g90	2.6 ± 0.3	42 ± 2	72 ± 2	3.7 ± 0.3	5.3 ± 2	114 ± 2	51 ± 3	162 ± 8
190	2.6 ± 0.3	37 ± 7	65 ± 8	5 ± 1	2.6 ± 0.3	103 ± 14	48 ± 5	140 ± 30
g86	2.2 ± 0.1	39 ± 8	56 ± 1	3.6 ± 0.1	3 ± 0.8	96 ± 9	56 ± 8	120 ± 10
g80	2.2 ± 0.4	46 ± 5	51 ± 8	3.2 ± 0.3	2 ± 0.5	95 ± 2	70 ± 7	80 ± 10

¹Three replicates were performed for each sample and the values reported are the averages and standard deviations for each set ²Post-yield stress drop was taken as the difference in the yield stress and the minimum in the stress after the yield point ³Strain hardening modulus, G_R , was taken as the slope of the stress-strain curve in the strain hardening regime, $\varepsilon > 20\%$.

Composition appears to affect the mechanical properties of the pre-strained polymers similar to the as-pressed polymers, where an increase in rubber content decreases the modulus and increases the strain at break. However, the toughness of the pre-strained polymers is largely invariant as the rubber content increases, in contrast to the trends in the as-pressed samples. This trend in toughness is largely due to the fact that the 100% PLA samples have an a_b similar to those of the BCPs when pre-strained. While a_b for the pre-strained polymers differs by less than a factor of two between all compositions, a_b for the as-pressed samples varied by over 50 times. Molecular architecture (e.g., 190 vs g90) only has a small effect on the yielding behavior of the pre-strained polymers, where the graft polymer has a higher yield stress and a larger post-yield stress drop than the linear counterpart.

The pre-strained samples appear to deform by homogeneous shear yielding up to the point of rupture. This behavior is qualitatively different than the deformation behavior displayed by the as-pressed samples, where the samples either necked before shear yielding (short t_a regime 1) or

crazed (intermediate and long t_a regimes 2 and 3). Although the deformation of the pre-strained polymers does not mimic the necking of the samples in regime 1, it does resemble the deformation of the as-pressed samples in the short t_a regime 1 at high strain (>200%). After the as-pressed (regime 1) polymers are fully cold drawn they strain harden, shear yielding uniformly across the entire tensile specimen until failure by rupture. In effect, the pre-strained samples bypass the cold drawing process and transition directly to the strain hardening regime.

The uniform deformation of the pre-strained samples indicates that the samples have eliminated strain localization. This is consistent with the minimization of strain softening, which has been shown to be severely reduced or eliminated with mechanical pre-straining. $^{60,85-88}$ Wu and van der Giessen demonstrated in numerical simulations that strain softening can be suppressed if the intrinsic strain hardening tendency is high enough to overcome the strain softening, 87 a result that has been extensively corroborated experimentally. 86,88,89 The strain hardening is much greater in the pre-strained samples as evidenced by the immediate transition to the strain hardening regime after yielding and the increase in the strain hardening modulus (G_R).

Aging of the pre-strained polymers was tested in a manner similar to the as-pressed samples, where the polymers were pre-strained and then aged for different t_a at ambient conditions. The aging time was taken as the time between pre-straining and uniaxial strain to break testing. Figure 13 shows the engineering stress-strain curves for the pre-strained g90 polymer aged for different times (data for all the polymers are shown in Figure S15) and the averaged results for the mechanical properties are summarized in Table 4 (results are plotted in Figure S16). The tensile properties (modulus, yield stress, strain at break, tensile strength, and toughness) of pre-strained g90 do not appreciably change with time, in contrast to the as-pressed material. For comparison, Figure 13 includes the embrittled as-pressed g90 that was aged for 21 days (blue dashed line). The

pre-strained g90 remained ductile for at least three times as long as the as-pressed samples, up to 60 days. In fact, all of the pre-strained polymers exhibited this persistence of ductility; even the 100% PLA samples (Figure S15A-B), which originally embrittled in 1 day, remained ductile after aging under ambient conditions for 60 days. Razavi and Wang also recently reported on the apparent permanent persistence of ductility in amorphous poly(L-lactide) that was pre-strained above $T_{\rm g}$. 84

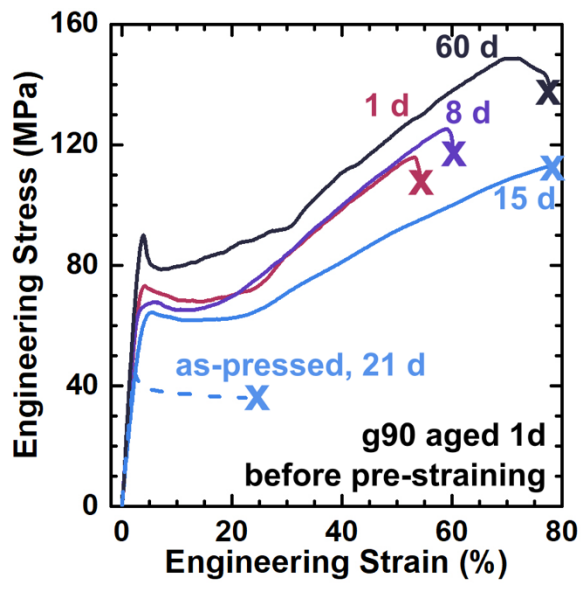


Figure 13. Tensile properties of pre-strained g90 as a function of aging time (all replicates shown in Figure S14). Samples were aged for 1 day at ambient conditions, pulled to 200% strain, and then aged again under ambient conditions (aging time labeled on the graph) before tensile testing. The dashed blue line shows the as-pressed g90 sample aged 21 days for comparison.

Table 4. Mechanical properties of pre-strained g90 as a function of aging time¹

t _a (days)	E (GPa)	Toughness (MJ/m³)	σ _y (MPa)	<i>E</i> _y (%)	PYSD ² (MPa)	σ _b (MPa)	& (%)	G _R ³ (MPa)
1	2.6 ± 0.2	42 ± 2	72 ± 3	3.7 ± 0.3	5 ± 2	115 ± 2	51 ± 3	153 ± 41
8	2.3 ± 0.4	45 ± 6	64 ± 3	4.6 ± 0.8	4 ± 1	110 ± 12	58 ± 2	137 ± 25
15	2.1 ± 0.4	51 ± 9	64 ± 4	4.4 ± 0.7	5 ± 1	108 ± 6	66 ± 9	121 ± 13
60	2.7 ± 0.5	66 ± 29	77 ± 9	4.1 ± 0.4	9 ± 1	117 ± 3	72 ± 28	125 ± 30

¹Three replicates were performed for each sample and the values reported are the averages and standard deviations for each set ²Post-yield stress drop was taken as the difference in the yield

stress and the minimum in the stress after the yield point 3 Strain hardening modulus, G_{R} , was taken as the slope of the stress-strain curve in the strain hardening regime, $\varepsilon > 20\%$.

Previous literature has shown that mechanically pre-strained polymers can reset the aging clock, where mechanical deformation acts like thermal treatment for physical aging. 48,49,60,90-92 Referred to as "mechanical rejuvenation," this process brings the polymer to a metastable, relatively high free volume state; releasing the mechanical strain is analogous to quenching thermally rejuvenated polymers and triggers structural relaxation of the polymer chains, where post-rejuvenation densification of the polymer melt increases segment-segment interactions. Structural relaxation is evidenced by an increase in the yield stress with aging time, which is observed for both thermally 56,94 and mechanically rejuvenated materials. 48,49 The pre-strained polymers in this report display a slight increase in yield stress with aging. However, the pre-strained polymers show no change in deformation mechanism, which for the as-pressed samples is the most reliable predictor of physical aging embrittlement. These observations suggest that the pre-strained polymers undergo some structural relaxation but that physical aging does not result in embrittlement of the samples on the timescales studied.

Densification of polymer chains is not the only factor dictating the potential energy landscape that ultimately determines whether polymers will embrittle after aging, as discussed in section 3.5. Mechanical deformation of the glassy structure can also alter this landscape and can also change the dominant deformation mechanism observed. Although direct measurement of the potential energy landscape or the glassy state of a polymer is not experimentally feasible, these concepts have been the subject of many simulation and theoretical analyses and have been used to interpret experimental results. Bending and Hebert observed an increase in the molecular mobility of deformed glassy polymers and demonstrated that the deformation induced rejuvenation of the

glasses. 46,92 They interpreted their results, with evidence from Chen and Schweizer's theory, 42,95 such that the basins of the potential energy landscapes rise with strain and that the barrier between energy minima is decreased to the point that it can be overcome by thermal perturbations. We propose that the glassy structure of our pre-strained polymers have transitioned to a new energetic minimum and that the shear stress in the new potential energy landscape is much lower than the craze stress, such that even aging of the glass will not alter the dominant deformation mechanism. Given the stability of the ductility and toughness of the pre-strained polymers—even the 100% PLA polymers that, as-pressed, embrittle within 1 day—we speculate that the mechanically rejuvenated polymers described here will not embrittle upon further aging.

It is important to note that while composition does not appear to be an important factor in the aging kinetics of the pre-strained polymers, it is a critical parameter for their preparation. The polymers have to be pre-strained within the short t_a regime such that they can be strained to 200%. The time frame over which regime 1 is operative is highly dependent on the rubber content: g100 transitions to the intermediate t_a regime 2 within about 1 hour whereas g80 remains in regime 1 for almost 200 days. In effect, the polymer composition and architecture can be used to tune the processing window of the polymer.

3.7 Shape memory properties

The processing of our PLA containing polymers has been demonstrated to be a critical design variable in controlling their resulting mechanical properties, where mechanical rejuvenation of polymers at short annealing times has been shown to be the best method for producing durable, tough PLA plastics. However, it was unclear if these mechanically rejuvenated polymers are permanently altered or whether they could be reprocessed similar to other thermally rejuvenated polymers, which is crucial for recycling or repurposing of polymer materials.

Figure 14 shows the behavior of g90 at various stages of heating and straining. First the polymer was aged 1 day and pre-strained resulting in the now established short t_a regime 1 behavior, i.e., yielding in a single step and cold drawing to 200% strain. The polymer was aged for 1 day at ambient conditions, then heated to 80 °C for 15 seconds. Heating the extended tensile bar led to rapid quantitative recovery of the original shape, reforming into a dog bone. The sample was again aged 1 day at ambient conditions, mirroring the initial aging conditions. A subsequent strain to break experiment yielded the same tensile behavior as the original as-pressed sample: regime 1 yielding with high ductility. This recovery of initial mechanical properties, or shape memory behavior, was observed for all of the polymers, including g100 and l100, as shown in Figure S17.

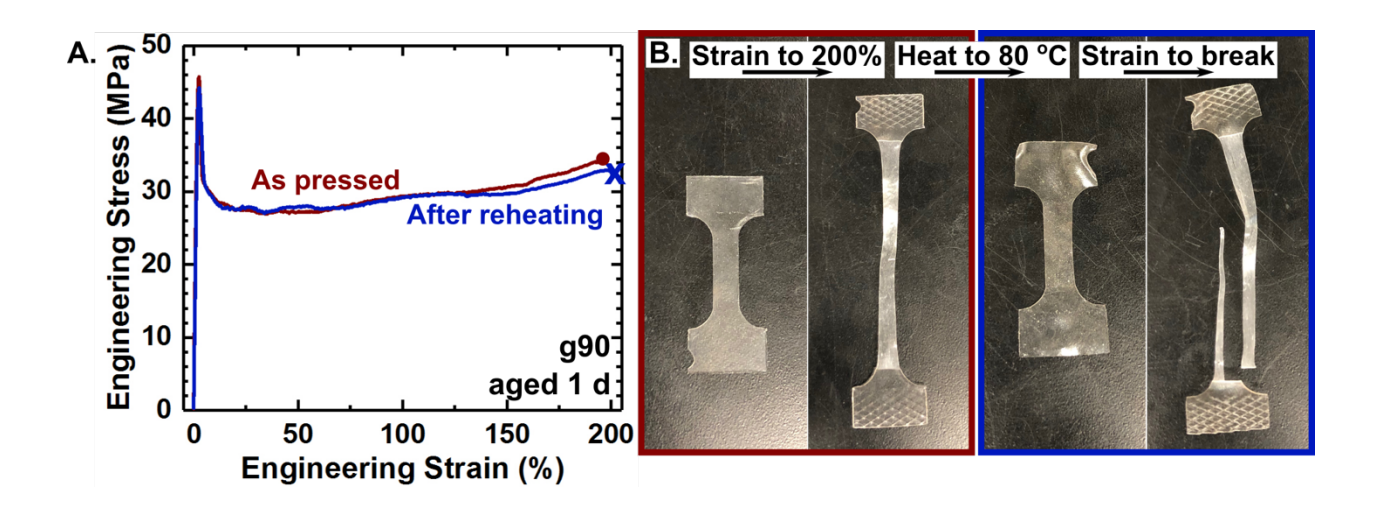


Figure 14. A. Tensile properties of g90 after hot pressing and aging 1 day at ambient conditions and stretched to 200% strain (as pressed, red curve) and after heating to 80 °C and aging 1 day at ambient conditions and strained to break (after reheating, blue curve). B. Photos of the tensile bar after hot pressing and pre-straining (red box) and photos of the tensile bar after it was heated to 80 °C and subsequently strained to break (blue box).

In addition to the recovery of the polymer's original mechanical properties, the reformed samples recovered the intermediate (regime 2) and long t_a (regime 3) behavior. After the shape memory process, when aged 3 days g90 develops a double yield and when aged more than 21 days

it is brittle (Figure S18). This demonstrates that the structure introduced by mechanical rejuvenation can be completely erased and that the plastic returns to the same potential energy landscape as when thermally pressed. Interestingly, aging of the pre-strained polymers did not affect the shape memory effect of the polymers. Full shape recovery was observed for pre-strained samples of all compositions that were aged for only 1 day and for samples that were aged 180 days after pre-straining. These results suggest that the two states, thermally and mechanically rejuvenated, are independent from each other and that switching between them is reversible. This demonstrates the universality of the rejuvenation processes, which raises the floor of the potential energy landscape, allowing the material to transition into new energy minima, and aging deepens the potential energy wells, resulting in the mechanical properties that we observe.

4 Conclusions

We have demonstrated that glassy PLA based graft BCPs containing between 10 and 20% of microphase separated rubbery P4MCL result in materials with dramatically delayed aging characteristics relative to pure PLA. These materials undergo physical aging, transforming from a ductile state immediately after thermal processing to a brittle material following an aging time t_a^* . Both the rubber modified BCPs and pure PLA display the same pattern of mechanical response with aging. At short t_a , denoted regime 1, the polymers are ductile, yielding in a single step followed by shear yielding. In regime 2, at intermediate t_a , the polymers deform in two yielding steps, which we suggest are first by crazing then by shear yielding. At long t_a , regime 3, the polymers yield then fail in a brittle fashion following crazing. Although the materials exhibit the same aging pattern, the time to brittle failure is strongly dependent on the composition. Pure linear and graft PLA embrittle in less than 2 days while a graft block copolymer containing 20% rubber remains ductile after 210 days at ambient conditions. Characterization of the deformation

mechanisms using TEM and SAXS suggests that crazing is initiated by rubber particle cavitation in regime 2 and 3, but the PLA fibrils rupture in regime 3, due to embrittlement of the material. DSC analysis confirms that the presence of the rubber slows aging but indicates that structural relaxation of the glassy PLA is not solely responsible for the evolution of the mechanical properties with t_a . We also demonstrated that pre-straining the pure PLA and graft BCPs while in regime 1 imposes mechanical rejuvenation, resulting in plastics with enhanced yield stress, tensile strength, and toughness, which persists for at least 60 days after processing. These mechanically pre-strained polymers form a modified glassy structure with a potential energy landscape more favorable to shear yielding, which results in ductility. Finally, the pre-strained polymers exhibit complete shape memory behavior, recovering the initial dog bone shape and original as-pressed mechanical properties after heating for several seconds above T_g . This shape memory behavior highlights the reversibility of each processing method and has important implications for potential applications such as shrink wrap labels for food and beverage containers.

5 Associated content

Supporting Information

Synthetic details, molecular characterization, and additional data. The Supporting Information is available free of charge on the ACS Publication website at DOI: 10.1021/acsmacromol.XXXXXXXX.

6 Notes

All primary data files are available at DOI:10.13020/0ym0-th31. The authors declare no competing financial interests.

7 Acknowledgements

This work was funded by the NSF through the Center for Sustainable Polymers CHE-1901635. This research used resources of the Advanced Photon Source APS), a U.S. Department of Energy DOE) Office of Science User Facility operated for the DOE Office of Science by Argonne National Laboratory under Contract DE-AC02-06CH11357. Part of this work was performed at the DuPont-Northwestern-Dow Collaborative Access Team DND-CAT) located at Sector 5 of the APS. DND-CAT is supported by E.I. DuPont de Nemours & Co., The Dow Chemical Company, and Northwestern University. Parts of this work were carried out in the Characterization Facility, University of Minnesota, which receives partial support from NSF through the MRSEC program.

8 References

- (1) The New Plastics Economy: Rethinking the Future of Plastics. World Economic Forum, Ellen MacArthur Foundation, and McKinsey and Company. The New Plastics Economy: Rethinking the Future of Plastics, 2016; http://www.ellenmacarthurfoundation.org/publications.
- (2) Hopewell, J.; Dvorak, R.; Kosior, E. Plastics Recycling: Challenges and Opportunities. *Philosophical Transactions of the Royal Society B: Biological Sciences* **2009**, *364* (1526), 2115–2126.
- (3) Rist, S.; Hartmann, N. B. *Aquatic Ecotoxicity of Microplastics and Nanoplastics:* Lessons Learned From Engineered Nanomaterials; Springer, Cham, 2017; Vol. 58.
- (4) Schneiderman, D. K.; Hillmyer, M. A. 50th Anniversary Perspective: There Is a Great Future in Sustainable Polymers. *Macromolecules* **2017**, *50* (10), 3733–3749.
- (5) Tokiwa, Y.; Calabia, B.; Ugwu, C.; Aiba, S. Biodegradability of Plastics. *IJMS* **2009**, *10* (9), 3722–3742.
- (6) Datta, R.; Henry, M. Lactic Acid: Recent Advances in Products, Processes and Technologies a Review. *J. Chem. Technol. Biotechnol.* **2006**, *81* (7), 1119–1129.
- (7) Drumright, R. E.; Gruber, P. R.; Henton, D. E. Polylactic Acid Technology. *Adv. Mater.* **2000**, *12*, 1841–1846.
- (8) Pan, P.; Zhu, B.; Inoue, Y. Enthalpy Relaxation and Embrittlement of Poly(L-Lactide) During Physical Aging. *Macromolecules* **2007**, *40* (26), 9664–9671.
- (9) Struik, L. C. E. Physical Aging in Plastics and Other Glassy Materials. *Polym. Eng. Sci.* **1977**, *17*, 165–173.
- (10) Hodge, I. M. Enthalpy Relaxation and Recovery in Amorphous Materials. *Journal of Non-Crystalline Solids* **1994**, *169*, 211–266.
- (11) Hutchinson, J. M. Physical Aging of Polymers. *Prog. Polym. Sci.* **1995**, *20*, 703–760.

- (12) Ren, J.; Urakawa, O.; Adachi, K. Dielectric and Viscoelastic Studies of Segmental and Normal Mode Relaxations in Undiluted Poly(*D*,*L*-Lactic Acid). *Macromolecules* **2003**, *36* (1), 210–219.
- (13) Chen, K.; Schweizer, K. S. Molecular Theory of Physical Aging in Polymer Glasses. *Phys. Rev. Lett.* **2007**, *98* (16), 167802–167804.
- (14) Chen, K.; Schweizer, K. S. Theory of Physical Aging in Polymer Glasses. *Phys. Rev. E* **2008**, 78 (3), 394–15.
- (15) Chen, K.; Saltzman, E. J.; Schweizer, K. S. Segmental Dynamics in Polymers: From Cold Melts to Ageing and Stressed Glasses. *J Phys Condens Matter* **2009**, *21* (50), 503101–503121.
- Osborne, M. J.; Lacks, D. J. Inherent Structure Analysis of the Thermal History Dependence of Yielding in Glasses † *J. Phys. Chem. B* **2004**, *108* (51), 19619–19622.
- (17) Lacks, D. J.; Osborne, M. J. Energy Landscape Picture of Overaging and Rejuvenation in a Sheared Glass. *Phys. Rev. Lett.* **2004**, *93* (25), 983–984.
- (18) Theryo, G. C. Deformation and Physical Aging of Rubber-Modified Polylactide Graft Copolymers, 2014, pp 1–210.
- (19) Liu, H.; Zhang, J. Research Progress in Toughening Modification of Poly(Lactic Acid). *J. Polym. Sci. B Polym. Phys.* **2011**, *49* (15), 1051–1083.
- (20) Anderson, K.; Schreck, K.; Hillmyer, M. Toughening Polylactide. *Polymer Reviews* **2008**, *48* (1), 85–108.
- Wu, N.; Zhang, H.; Fu, G. Super-Tough Poly(Lactide) Thermoplastic Vulcanizates Based on Modified Natural Rubber. *ACS Sustainable Chem. Eng.* **2016**, *5* (1), 78–84.
- Wu, N.; Zhang, H. Mechanical Properties and Phase Morphology of Super-Tough PLA/PBAT/EMA-GMA Multicomponent Blends. *Materials Letters* **2017**, *192*, 17–20.
- Sun, Y.; He, C. Biodegradable "Core–Shell" Rubber Nanoparticles and Their Toughening of Poly(Lactides). *Macromolecules* **2013**, *46* (24), 9625–9633.
- Wanamaker, C. L.; O'Leary, L. E.; Lynd, N. A.; Hillmyer, M. A.; Tolman, W. B. Renewable-Resource Thermoplastic Elastomers Based on Polylactide and Polymenthide. *Biomacromolecules* **2007**, *8* (11), 3634–3640.
- (25) Kulinski, Z.; Piorkowska, E. Crystallization, Structure and Properties of Plasticized Poly(L-Lactide). *Polymer* **2005**, *46* (23), 10290–10300.
- (26) Kowalczyk, M.; Piorkowska, E. Mechanisms of Plastic Deformation in Biodegradable Polylactide/Poly(1,4-Cis-Isoprene) Blends. *J. Appl. Polym. Sci.* **2012**, *124*, 4579–4589.
- (27) Schneiderman, D. K.; Hill, E. M.; Martello, M. T.; Hillmyer, M. A. Poly(Lactide)-Block-Poly(E-Caprolactone-Co-E-Decalactone)-Block-Poly(Lactide) Copolymer Elastomers. *Polym. Chem.* **2015**, *6* (19), 3641–3651.
- (28) Martello, M. T.; Hillmyer, M. A. Polylactide–Poly(6-Methyl-E-Caprolactone)–Polylactide Thermoplastic Elastomers. *Macromolecules* **2011**, *44* (21), 8537–8545.
- (29) Frick, E. M.; Zalusky, A. S.; Hillmyer, M. A. Characterization of Polylactide-B-Polyisoprene-B-Polylactide Thermoplastic Elastomers. *Biomacromolecules* **2003**, *4* (2), 216–223.
- (30) Watts, A.; Kurokawa, N.; Hillmyer, M. A. Strong, Resilient, and Sustainable Aliphatic Polyester Thermoplastic Elastomers. *Biomacromolecules* **2017**, *18* (6), 1845–1854.
- (31) López-Rodríguez, N.; López-Arraiza, A.; Meaurio, E.; Sarasua, J. R. Crystallization, Morphology, and Mechanical Behavior of Polylactide/Poly(E-Caprolactone) Blends. *Polym. Eng. Sci.* **2006**, *46* (9), 1299–1308.

- (32) Jing, F.; Hillmyer, M. A. A Bifunctional Monomer Derived From Lactide for Toughening Polylactide. *J. Am. Chem. Soc.* **2008**, *130* (42), 13826–13827.
- (33) Zhang, J.; Schneiderman, D. K.; Li, T.; Hillmyer, M. A.; Bates, F. S. Design of Graft Block Polymer Thermoplastics. *Macromolecules* **2016**, *49* (23), 9108–9118.
- Zhang, J.; Li, T.; Mannion, A. M.; Schneiderman, D. K.; Hillmyer, M. A.; Bates, F. S. Tough and Sustainable Graft Block Copolymer Thermoplastics. *ACS Macro Lett.* **2016**, 5 (3), 407–412.
- (35) Haugan, I. N.; Maher, M. J.; Chang, A. B.; Lin, T.-P.; Grubbs, R. H.; Hillmyer, M. A.; Bates, F. S. Consequences of Grafting Density on the Linear Viscoelastic Behavior of Graft Polymers. *ACS Macro Lett.* **2018**, 525–530.
- (36) Dalsin, S. J.; Hillmyer, M. A.; Bates, F. S. Molecular Weight Dependence of Zero-Shear Viscosity in Atactic Polypropylene Bottlebrush Polymers. *ACS Macro Lett.* **2014**, *3* (5), 423–427.
- (37) Cugini, A. V.; Lesser, A. J. Aspects of Physical Aging, Mechanical Rejuvenation, and Thermal Annealing in a New Copolyester. *Polym. Eng. Sci.* **2014**, *55* (8), 1941–1950.
- (38) Ricco, T.; Smith, T. L. Rejuvenation and Physical Ageing of a Polycarbonate Film Subjected to Finite Tensile Strains*. *Polymer* **1985**, *26*, 1979–1985.
- (39) Lyulin, A. V.; Michels, M. A. J. Time Scales and Mechanisms of Relaxation in the Energy Landscape of Polymer Glass Under Deformation: Direct Atomistic Modeling. *Phys. Rev. Lett.* **2007**, *99* (8), 085504–085504.
- (40) Jatin; Sudarkodi, V.; Basu, S. Investigations Into the Origins of Plastic Flow and Strain Hardening in Amorphous Glassy Polymers. *International Journal of Plasticity* **2014**, *56* (C), 139–155.
- (41) Chen, K.; Schweizer, K. S. Microscopic Constitutive Equation Theory for the Nonlinear Mechanical Response of Polymer Glasses. *Macromolecules* **2008**, *41* (15), 5908–5918.
- (42) Chen, K.; Schweizer, K. S. Theory of Aging, Rejuvenation, and the Nonequilibrium Steady State in Deformed Polymer Glasses. *Phys. Rev. E* **2010**, *82* (4), 376–12.
- (43) Lee, H.-N.; Paeng, K.; Swallen, S. F.; Ediger, M. D. Direct Measurement of Molecualr Mobility in Actively Deformed Polymer Glasses. *Science* **2009**, *323* (5911), 231–234.
- (44) Kalfus, J.; Detwiler, A.; Lesser, A. J. Probing Segmental Dynamics of Polymer Glasses During Tensile Deformation with Dielectric Spectroscopy. *Macromolecules* **2012**, *45* (11), 4839–4847.
- (45) Bending, B.; Ediger, M. D. Comparison of Mechanical and Molecular Measures of Mobility During Constant Strain Rate Deformation of a PMMA Glass. *J. Polym. Sci. B Polym. Phys.* **2016**, *54* (19), 1957–1967.
- (46) Bending, B.; Christison, K.; Ricci, J.; Ediger, M. D. Measurement of Segmental Mobility During Constant Strain Rate Deformation of a Poly(Methyl Methacrylate) Glass. *Macromolecules* **2014**, *47* (2), 800–806.
- (47) Utz, M.; Debenedetti, P. G.; Stillinger, F. H. Atomistic Simulation of Aging and Rejuvenation in Glasses. *Phys. Rev. Lett.* **2000**, *84*, 1471–1474.
- van Melick, H. G. H.; Govaert, L. E.; Raas, B.; Nauta, W. J.; Meijer, H. E. H. Kinetics of Ageing and Re-Embrittlement of Mechanically Rejuvenated Polystyrene. *Polymer* **2003**, *44*, 1171–1179.
- (49) Kierkels, J. T. A.; Dona, C. L.; Tervoort, T. A.; Govaert, L. E. Kinetics of Re-Embrittlement of (Anti)Plasticized Glassy Polymers After Mechanical Rejuvenation. *J. Polym. Sci. B Polym. Phys.* **2007**, *46* (2), 134–147.

- (50) Liu, Q.; Zhang, H.; Zhu, M.; Dong, Z.; Wu, C.; Jiang, J.; Li, X.; Luo, F.; Gao, Y.; Deng, B.; Zhang, Y.; Xing, J.; Wang, H.; Li, X. Blends of Polylactide/Thermoplactic Elastomer: Miscibility, Physical Aging and Crystallization Behaviors. *Fibers Polym* **2013**, *14* (10), 1688–1698.
- (51) Maher, M. J.; Schibur, H. J.; Bates, F. S. When Convergent Syntheses of Graft Block Copolymers Diverge: the Treachery of Chemical Images. *J. Polym. Sci. A Polym. Chem.* **2017**, *55* (18), 3097–3104.
- (52) De Hoe, G. X.; Zumstein, M. T.; Tiegs, B. J.; Brutman, J. P.; McNeill, K.; Sander, M.; Coates, G. W.; Hillmyer, M. A. Sustainable Polyester Elastomers From Lactones: Synthesis, Properties, and Enzymatic Hydrolyzability. *J. Am. Chem. Soc.* **2018**, *140* (3), 963–973.
- (53) Maher, M. J.; Jones, S. D.; Zografos, A.; Xu, J.; Schibur, H. J.; Bates, F. S. The Order–Disorder Transition in Graft Block Copolymers. *Macromolecules* **2017**, *51* (1), 232–241.
- (54) Theryo, G.; Jing, F.; Pitet, L. M.; Hillmyer, M. A. Tough Polylactide Graft Copolymers. *Macromolecules* **2010**, *43* (18), 7394–7397.
- (55) Collyer, A. A. *Rubber Toughened Engineering Plastics*; Chapman and Hall: London, UK, 1994.
- (56) Struik, L. C. E. *Physical Aging in Polymers and Other Amorphous Materials*; Elsevier: Amsterdam.
- (57) Ruokolainen, J.; Fredrickson, G. H.; Kramer, E. J.; Ryu, C. Y.; Hahn, S. F.; Magonov, S. N. Effect of Thermal History and Microdomain Orientation on Deformation and Fracture Properties of Poly(Cyclohexylethylene)—Polyethylene Triblock Copolymers Containing Cylindrical PE Domains. *Macromolecules* **2002**, *35* (25), 9391–9402.
- van Melick, H. G. H.; Govaert, L. E.; Meijer, H. E. H. Localisation Phenomena in Glassy Polymers: Influence of Thermal and Mechanical History. *Polymer* **2003**, *44* (12), 3579–3591.
- (59) Meijer, H. E. H.; Govaert, L. E. Mechanical Performance of Polymer Systems: the Relation Between Structure and Properties. *Progress in Polymer Science* **2005**, *30* (8-9), 915–938.
- (60) Hasan, O. A.; Boyce, M. C. Energy Storage During Inelastic Deformation of Glassy Polymers. *Polymer* **1993**, *34*, 5085–5092.
- (61) Bucknall, C. B. Quantitative Approaches to Particle Cavitation, Shear Yielding, and Crazing in Rubber-Toughened Polymers. *J. Polym. Sci. B Polym. Phys.* **2007**, *45* (12), 1399–1409.
- Jang, B. Z.; Uhlmann, D. R.; Vander Sande, J. B. The Rubber Particle Size Dependence of Crazing in Polypropylene. *Polym. Eng. Sci.* **2004**, *25*, 643–651.
- (63) Kim, G.-M.; Michler, G. H. Micromechanical Deformation Processes in Toughened and Particle Filled Semicrystalline Polymers. Part 2: Model Representation for Micromechanical Deformation Processes. *Polymer* **1998**, *39*, 5699–5703.
- (64) Wu, S. Generalized Criterion for Rubber Toughening: the Critical Matrix Ligament Thickness. *J. Appl. Polym. Sci.* **1988**, *35*, 549–561.
- (65) Dompas, D.; Groeninckx, G. Toughening Behaviour of Rubber-Modified Thermoplastic Polymers Involving Very Small Rubber Particles: 1. a Criterion for Internal Rubber Cavitation. *Polymer* **1994**, *35*, 4743–4749.
- (66) Argon, A. S.; Cohen, R. E.; Gebizlioglu, O. S.; Schwier, C. E. Crazing in Block Copolymers and Blends. *Advances in Polymer Science* **1983**, 275–334.

- (67) Suzuki, S.; Nishitsuji, S.; Inoue, T. Physical Aging and Thermal Aging Resistance of Polycarbonate/Poly(Styrene-B-(Ethylene-Co-Butylene)-B-Styrene) Blends. *Polym. Eng. Sci.* **2012**, *52* (9), 1958–1963.
- (68) DiCorleto, J. A.; Cohen, R. E. Physical Ageing and Toughness of Diblock Copolymers. *Polymer* **2002**, *29*, 1245–1254.
- (69) Zhang, Z.; Zhao, X.; Wang, S.; Zhang, J.; Zhang, W. Inducing a Network Structure of Rubber Phase: an Effective Approach to Toughen Polymer Without Sacrificing Stiffness. *RSC Advances* **2014**, *4* (105), 60617–60625.
- (70) Schwier, C. E.; Argon, A. S.; Cohen, R. E. Craze Plasticity in a Series of Polystyrene/Polybutadiene Di-Block Copolymers with Spherical Morphology. *Philosophical Magazine A* **1985**, *52*, 581–603.
- (71) Schwier, C. E.; Argon, A. S.; Cohen, R. E. Crazing in Polystyrene-Polybutadiene Diblock Copolymers Containing Cylindrical Polybutadiene Domains. *Polymer* **1985**, *26*, 1985–1993.
- (72) Stoclet, G.; Lefebvre, J. M.; Seguela, R.; Vanmansart, C. In-Situ SAXS Study of the Plastic Deformation Behavior of Polylactide Upon Cold-Drawing. *Polymer* **2014**, *55* (7), 1817–1828.
- (73) Brown, H.; Kramer, E. Craze Microstructure From Small-Angle X-Ray Scattering. *Journal of Macromolecular Science-Physics* **1981**, *B19*, 487–522.
- (74) Salomons, G. J.; Singh, M. A.; Bardouille, T.; Foran, W. A.; Capel, M. S. Small-Angle X-Ray Scattering Analysis of Craze-Fibril Structures. *Journal of Applied Crystallography* **1999**, *32*, 71–81.
- (75) Declet-Perez, C.; Francis, L. F.; Bates, F. S. Cavitation in Block Copolymer Modified Epoxy Revealed by in Situ Small-Angle X-Ray Scattering. *ACS Macro Lett.* **2013**, *2* (10), 939–943.
- (76) Hutchinson, J. M.; Smith, S.; Horne, B.; Gourlay, G. M. Physical Aging of Polycarbonate: Enthalpy Relaxation, Creep Response, and Yielding Behavior. *Macromolecules* **1999**, *32* (15), 5046–5061.
- (77) Nimmer, R. M. An Analytic Study of Tensile and Puncture Test Behavior as a Function of Large-Strain Properties. *Polym. Eng. Sci.* **1987**, 263–270.
- (78) Zhao, X.; Ye, L.; Coates, P.; Caton-Rose, F.; Martyn, M. Structure and Blood Compatibility of Highly Oriented Poly(Lactic Acid)/Thermoplastic Polyurethane Blends Produced by Solid Hot Stretching. *Polym. Adv. Technol.* **2013**, *24* (9), 853–860.
- (79) Chen, Y.; Han, L.; Li, Z.; Kong, J.; Wu, D.; Cao, Z.; Dong, L. Effect of Uniaxial Pre-Stretching on the Microstructure and Mechanical Properties of Poly[(Ethylene Oxide)-Block-(Amide-12)]-Toughened Poly(Lactic Acid) Blend. *RSC Advances* **2016**, *7*, 712–719.
- (80) Jariyasakoolroj, P.; Tashiro, K.; Wang, H.; Yamamoto, H.; Chinsirikul, W.; Kerddonfag, N.; Chirachanchai, S. Isotropically Small Crystalline Lamellae Induced by High Biaxial-Stretching Rate as a Key Microstructure for Super-Tough Polylactide Film. *Polymer* **2015**, *68* (C), 234–245.
- (81) Bobovitch, A. L.; Tkach, R.; Ajji, A.; Elkoun, S.; Nir, Y.; Unigovski, Y.; Gutman, E. M. Mechanical Properties, Stress-Relaxation, and Orientation of Double Bubble Biaxially Oriented Polyethylene Films. *J. Appl. Polym. Sci.* **2006**, *100* (5), 3545–3553.

- (82) Wu, J.-H.; Yen, M.-S.; Wu, C.-P.; Li, C.-H.; Kuo, M. C. Effect of Biaxial Stretching on Thermal Properties, Shrinkage and Mechanical Properties of Poly (Lactic Acid) Films. *Journal of Polymers and the Environment* **2012**, *21* (1), 303–311.
- (83) Velazquez-Infante, J. C.; Gamez-Perez, J.; Franco-Urquiza, E. A.; Santana, O. O.; Carrasco, F.; Ll Maspoch, M. Effect of the Unidirectional Drawing on the Thermal and Mechanical Properties of PLA Films with Different L-Isomer Content. *J. Appl. Polym. Sci.* **2012**, *127* (4), 2661–2669.
- (84) Razavi, M.; Wang, S.-Q. Why Is Crystalline Poly(Lactic Acid) Brittle at Room Temperature? *Macromolecules* **2019**, *52* (14), 5429–5441.
- (85) Govaert, L. E.; van Melick, H. G. H.; Meijer, H. E. H. Temporary Toughening of Polystyrene Through Mechanical Pre-Conditioning. *Polymer* **2001**, *42*, 1271–1274.
- (86) Govaert, L. E.; Timmermans, P. H. M.; Brekelmans, W. A. M. The Influence of Intrinsic Strain Softening on Strain Localization in Polycarbonate: Modeling and Experimental Validation. *Journal of Engineering Materials and Technology* **2000**, *122*, 177–185.
- (87) Wu, P. D.; Van der Giessen, E. On Neck Propagation in Amorphous Glassy Polymers Under Plane Strain Tension. *International Journal of Plasticity* **1995**, *11*, 211–235.
- (88) G'Sell, C. Plastic Deformation of Glassy Polymers: Constitutive Equations and Macromolecular Mechanisms. in: McQueen H, Editor. Strength of Metals and Alloys.; Oxford: Perrgamon Press, 1986; pp 1943–1982.
- (89) Bauwens, J.-C. A New Approach to Describe the Tensile Stress-Strain Curve of a Glassy Polymer. *Journal of Materials Science* **1978**, *13*, 1443–1448.
- (90) Oyanguren, P. A.; Vallo, C. I.; Frontini, P. M.; Williams, R. J. J. Rejuvenation of Epoxy Glasses Subjected to Uniaxial Compression. *Polymer* **1994**, *35*, 5279–5283.
- (91) Martinez-Vega, J. J.; Trumel, H.; Gacougnolle, J. L. Plastic Deformation and Physical Ageing in PMMA. *Polymer* **2002**, *43*, 4979–4987.
- (92) Hebert, K.; Ediger, M. D. Reversing Strain Deformation Probes Mechanisms for Enhanced Segmental Mobility of Polymer Glasses. *Macromolecules* **2017**, *50* (3), 1016–1026.
- (93) McKenna, G. B. Mechanical Rejuvenation in Polymer Glasses: Fact or Fallacy? *J Phys Condens Matter* **2003**, *15* (11), S737–S763.
- (94) Hasan, O. A.; Boyce, M. C.; Li, X. S.; Berko, S. An Investigation of the Yield and Postyield Behavior and Corresponding Structure of Poly(Methyl Methacrylate). **1993**, *31*, 185–197.
- (95) Chen, K.; Schweizer, K. S. Theory of Yielding, Strain Softening, and Steady Plastic Flow in Polymer Glasses Under Constant Strain Rate Deformation. *Macromolecules* **2011**, *44* (10), 3988–4000.